

EPR Study of Vanadyl Complexes with  
Schiff Bases Derived from S-Methyl-  
Carbodithioato-Hydrazine

by

Al-Turabi Mohamed Omer Hamad

A Thesis Presented to the

FACULTY OF THE COLLEGE OF GRADUATE STUDIES

KING FAHD UNIVERSITY OF PETROLEUM & MINERALS

DHAHRAN, SAUDI ARABIA

In Partial Fulfillment of the  
Requirements for the Degree of

**MASTER OF SCIENCE**

In

**CHEMISTRY**

January, 1992

## INFORMATION TO USERS

This manuscript has been reproduced from the microfilm master. UMI films the text directly from the original or copy submitted. Thus, some thesis and dissertation copies are in typewriter face, while others may be from any type of computer printer.

**The quality of this reproduction is dependent upon the quality of the copy submitted.** Broken or indistinct print, colored or poor quality illustrations and photographs, print bleedthrough, substandard margins, and improper alignment can adversely affect reproduction.

In the unlikely event that the author did not send UMI a complete manuscript and there are missing pages, these will be noted. Also, if unauthorized copyright material had to be removed, a note will indicate the deletion.

Oversize materials (e.g., maps, drawings, charts) are reproduced by sectioning the original, beginning at the upper left-hand corner and continuing from left to right in equal sections with small overlaps. Each original is also photographed in one exposure and is included in reduced form at the back of the book.

Photographs included in the original manuscript have been reproduced xerographically in this copy. Higher quality 6" x 9" black and white photographic prints are available for any photographs or illustrations appearing in this copy for an additional charge. Contact UMI directly to order.

# U·M·I

University Microfilms International  
A Bell & Howell Information Company  
300 North Zeeb Road, Ann Arbor, MI 48106-1346 USA  
313/761-4700 800/521-0600



**Order Number 1354038**

**EPR study of vanadyl complexes with Schiff bases derived from  
S-methyl-carbodithioato-hydrazine**

**Al-Turabi, Mohamed Omer Hamad, M.S.**

**King Fahd University of Petroleum and Minerals (Saudi Arabia), 1992**

**U·M·I**  
300 N. Zeeb Rd.  
Ann Arbor, MI 48106



**EPR STUDY OF VANADYL COMPLEXES WITH  
SCHIFF BASES DERIVED FROM S-METHYL-  
CARBODITHIOATO-HYDRAZINE**

**BY**

**AL-TURABI MOHAMED OMER HAMAD**

**A Thesis Presented to the  
FACULTY OF THE COLLEGE OF GRADUATE STUDIES  
KING FAHD UNIVERSITY OF PETROLEUM & MINERALS  
DHAHRAN, SAUDI ARABIA**

**In Partial Fulfillment of the  
Requirements for the Degree of**

**MASTER OF SCIENCE**

**In**

**CHEMISTRY**

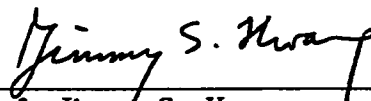
**JANUARY, 1992**

KING FAHD UNIVERSITY OF PETROLEUM AND MINERALS  
DHAHRAN, SAUDI ARABIA

COLLEGE OF GRADUATE STUDIES

This thesis, written by Mr. Mohamed Omer Hamad Al-Turabi under the direction of his Thesis Advisor and approved by his Thesis Committee, has been presented to and accepted by the Dean of the College of Graduate Studies, in partial fulfillment of the requirements for the degree of MASTER OF SCIENCE in Chemistry.

Thesis Committee:



Prof. Jimmy S. Hwang  
Thesis Advisor



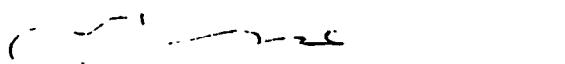
Dr. Abdul Rahman A. Al-Arfaj  
Member

A. Suwayan

Dr. Abdulaziz A. Al-Suwayyan  
Member



Dr. Abdulrahman H. Al-Husaini  
Department Chairman



Dr. Ala H. Al-Rabeh  
Dean, College of Graduate Studies

Date: 9. 2. 92

**This thesis is dedicated  
to my parents.**



## ACKNOWLEDGEMENT

Acknowledgment is due to King Fahd University of Petroleum and Minerals for extending all facilities and providing financial support, and to the Chemistry Department and its Chairman, Dr. Abdulrahman H. Al-Husaini for his help and encouragement throughout this research.

I would like to offer my indebtedness and sincere appreciation to my major advisor Prof. Jimmy S. Hwang, whom I can never thank enough for his great help and encouragement during this research. Prof. Hwang always made free access for me whenever I needed. I greatly appreciate the invaluable suggestions and co-operation extended by Dr. Abdul Rahman A. Al-Arfaj and Dr. Abdulaziz A. Al-Suwaiyan who served as members of thesis committee. Thanks are also due to Mr. Saleem for his assistance in the experimental part. Acknowledgement is also due to Prof. Laila Al-Sayed (Faculty of Science, Alexandria University) for providing me with the compounds. I also thank Mr. Yassir Babikir for his help during the time of this thesis.

I am also thankful to all faculty, colleagues and friends who made my stay at the University a memorable and valuable experience.

## TABLE OF CONTENTS

	Page
List of Tables . . . . .	i
List of Figures . . . . .	ii
Abstract - in Arabic . . . . .	iv
Abstract - in English . . . . .	v
 CHAPTER 1 . . . . .	 1
1.1 INTRODUCTION . . . . .	2
1.2 ELECTRON PARAMAGNETIC RESONANCE . . . . .	7
1.3 SPIN HAMILTONIAN AND DEFINITION OF THE PARAMETERS . . . . .	10
1.3.1 EPR Spectra in Solution . . . . .	10
1.3.2 EPR Spectra in the Absence of Molecular Motions	16
1.3.2.1 Anisotropic Effects . . . . .	16
1.3.2.2 The Effect of Rotational Motion on EPR Spectra	20
1.4 THE CORRELATION TIME GROUP . . . . .	21
1.5 MOLECULAR TUMBLING . . . . .	22
1.6 FAST TUMBLING . . . . .	24
 CHAPTER 2: APPARATUS . . . . .	 26
2.1 INTRODUCTION . . . . .	26
2.2 VARIAN E-109 EPR SPECTROMETER . . . . .	26
2.2.1 General Description . . . . .	26
2.2.2 Data Acquisition . . . . .	28

2.2.2.1	Introduction . . . . .	28
2.2.2.2	E-935 System Software . . . . .	29
2.2.2.3	Magnet Scan . . . . .	29
2.2.2.4	Data File Capability . . . . .	29
2.2.2.5	Data Manipulation . . . . .	30
2.2.2.6	Tape Cartridge and File System . . . . .	31
2.3	BRUKER ER-200P-SRC . . . . .	31
2.3.1	General Description . . . . .	31
2.3.2	The Microwave Bridge . . . . .	32
2.3.3	The Microwave Probe . . . . .	33
2.3.4	DATA System (ER140) . . . . .	33
2.4	THE BASIC EPR SPECTROMETER (FUNCTIONAL DESCRIPTION) . . . . .	34
2.5	VACUUM SYSTEM . . . . .	37
CHAPTER 3:	PROCEDURE . . . . .	38
3.1	SAMPLE PREPARATION . . . . .	38
3.1.1	VO[(CH <sub>3</sub> ) <sub>2</sub> C=NNC <sub>3</sub> SSCH <sub>3</sub> ] <sub>2</sub> . . . . .	38
3.1.2	VO[Sal SB](Phen) . . . . .	40
3.1.3	VO[5-MeO Sal SB](Phen) . . . . .	40
3.2	DATA COLLECTION . . . . .	42
3.2.1	EPR Spectrometer Operation . . . . .	42
3.2.2	Spetra Taking . . . . .	42

CHAPTER 4: RESULTS AND DISCUSSION . . . . .	45
4.1 DETERMINATION OF THE MAGNETIC PARAMETERS . . . . .	45
4.1.1 Isotropic Magnetic Parameters . . . . .	45
4.1.2 Anisotropic Magnetic Parameters . . . . .	50
4.2 MOTIONAL NARROWING ANALYSIS . . . . .	60
4.2.1 VO[(CH <sub>3</sub> ) <sub>2</sub> C=NNCSSH <sub>3</sub> ] <sub>2</sub> . . . . .	60
4.2.2 VO[5-MeO Sal SB](Phen). . . . .	74
4.3 ANISOTROPIC INTERACTION PARAMETER . . . . .	85
4.3.1 VO[(CH <sub>3</sub> ) <sub>2</sub> C=NNCSSH <sub>3</sub> ] <sub>2</sub> . . . . .	85
4.3.2 VO[5-MeO Sal SB](Phen). . . . .	89
4.4 STICKNESS FACTOR . . . . .	92
4.4.1 VO[(CH <sub>3</sub> ) <sub>2</sub> C=NNCSSH <sub>3</sub> ] <sub>2</sub> . . . . .	92
4.4.2 VO[5-MeO Sal SB](Phen). . . . .	96
4.5 STOKES-EINSTEIN MODEL . . . . .	98
4.6 ALLOWED-VALUES EQUATION . . . . .	102
CHAPTER 5: CONCLUSIONS . . . . .	105
REFERENCES . . . . .	108

6220

## LIST OF TABLES

Table	Page
4.1 The Isotropic Magnetic Parameters . . . . .	49
4.2 The Anisotropic Magnetic Parameters . . . . .	58
4.3 Isotropic $g$ and $A$ for $\text{VO}[(\text{CH}_3)_2\text{C}=\text{NNCSSCH}_3]_2$ in toluene. . . . .	59
4.4 $B$ and $C$ for $\text{VO}[(\text{CH}_3)_2\text{C}=\text{NNCSSCH}_3]_2$ in toluene. . .	65
4.5 $B$ and $C$ for $\text{VO}[5\text{-MeO Sal SB}] (\text{Phen})$ in methylene chloride. . . . .	78
4.6 $\tau_R$ and $\eta/T$ values for $\text{VO}[(\text{CH}_3)_2\text{C}=\text{NNCSSCH}_3]_2$ in toluene at different temperatures . . . . .	86
4.7 $\tau_R$ and $\eta/T$ Values for $\text{VO}[5\text{-MeO Sal SB}] (\text{Phen})$ at Different Temperatures in methylene chloride. . . . .	90

## LIST OF FIGURES

Figure		Page
1.1	Structure of Cis- $\text{VO}[(\text{CH}_3)_2\text{C}=\text{NNCSSCH}_3]_2$ . . . . .	2
1.2	Structure of Trans- $\text{VO}[(\text{CH}_3)_2\text{C}=\text{NNCSSCH}_3]_2$ . . . . .	2
1.3	Structure of $\text{VO}[\text{Sal SB}]$ (Phen) . . . . .	4
1.4	Structure of $\text{VO}[5\text{-MeO Sal SB}]$ (Phen) . . . . .	4
1.5	A typical X-band spectrum of Oxovanadium(IV) at room temperature with DPPH as internal standard . . . . .	15
1.6	A typical X-band spectrum of Oxovanadium(IV) at 77 K . . . . .	17
2.1	EPR System Pictorial Block Diagram . . . . .	35
2.2	Functional Block Diagram-ER Series Spectrometer . . . . .	36
4.1	X-band Spectrum of $\text{VO}[(\text{CH}_3)_2\text{C}=\text{NNCSSCH}_3]_2$ in toluene at room temperature with DPPH as internal standard . . . . .	46
4.2	X-band Spectrum of $\text{VO}[\text{Sal SB}]$ (Phen) in toluene at room temperature with DPPH as internal standard. . . . .	47
4.3	X-band Spectrum of $\text{VO}[5\text{-MeO Sal SB}]$ (Phen) in methylene chloride at room temperature with DPPH as internal standard. . . . .	48
4.4	X-band Spectrum of $\text{VO}[(\text{CH}_3)_2\text{C}=\text{NNCSSCH}_3]_2$ in toluene at $T = 77 \text{ K}$ . . . . .	51
4.5	X-band Spectrum of $\text{VO}[\text{Sal SB}]$ (Phen) in toluene at $T = 77 \text{ K}$ . . . . .	56
4.6	X-band Spectrum of $\text{VO}[5\text{-MeO Sal SB}]$ (Phen) in methylene chloride at $T = 77 \text{ K}$ . . . . .	57
4.7	Experimental Spectra of $\text{VO}[(\text{CH}_3)_2\text{C}=\text{NNCSSCH}_3]_2$ in toluene. . . . .	61
4.8	C vs. B (experimental) plot of $\text{VO}[(\text{CH}_3)_2\text{C}=\text{NNCSSCH}_3]_2$ in toluene at different temperatures . . . . .	66

4.9	Effect of varying N for $\text{VO}[(\text{CH}_3)_2\text{C}=\text{NNCSSCH}_3]_2$ in toluene. Curves are simulated with $\bar{Z} = \text{Y}$ . . . . .	70
4.10	Effect of varying N for $\text{VO}[(\text{CH}_3)_2\text{C}=\text{NNCSSCH}_3]_2$ in toluene. Curves are simulated with $\bar{Z} = \text{X}$ . . . . .	72
4.11	Effect of varying N for $\text{VO}[(\text{CH}_3)_2\text{C}=\text{NNCSSCH}_3]_2$ in toluene. Curves are simulated with $\bar{Z} = \text{Z}$ . . . . .	73
4.12	Experimental spectra of $\text{VO}[5\text{-MeO Sal SB}]$ (Phen) in methylene chloride. . . . .	75
4.13	C vs. B (experimental) plot of $\text{VO}[5\text{-MeO Sal SB}]$ (Phen) in methylene chloride at different temperatures. . . . .	79
4.14	Effect of varying N for $\text{VO}[5\text{-MeO Sal SB}]$ (Phen) in methylene chloride. Curves are simulated with $\bar{Z} = \text{Y}$ . . . . .	80
4.15	Effect of varying N for $\text{VO}[5\text{-MeO Sal SB}]$ (Phen) in methylene chloride. Curves are simulated with $\bar{Z} = \text{Z}$ . . . . .	82
4.16	Effect of varying N for $\text{VO}[5\text{-MeO Sal SB}]$ (Phen) in methylene chloride. Curves are simulated with $\bar{Z} = \text{X}$ . . . . .	83
4.17	$\tau_R$ vs $\eta/T$ plot for $\text{VO}[(\text{CH}_3)_2\text{C}=\text{NNCSSCH}_3]_2$ in toluene. . . . .	87
4.18	$\tau_R$ vs $\eta/T$ plot for $\text{VO}[5\text{-MeO Sal SB}]$ (Phen) in methylene chloride . . . . .	91

## الخلاصة

لقد تم دراسة عرض خط طيف طنين المغناطيسية المسايرة الالكتروني لنظامين من مركبات أكسى الفانديوم عند تردد الموجات الدقيقة البالغ قدرها ٩ جيجاهيرتز فى مدى الحركة السريعة . وأمكن تعيين كل من مدى تباين الدوران (N) ومعامل الزمن الدورانى ( $T_p$ ) . النظام الاول هو ثنائي - (S - ميثيل - ٢ - ايزوبروبيل - هايدرازين - كاربودايثيوتو) أكسى الفانديوم فى تولوين . بينما النظام الثانى هو S - ميثيل - N - ٥ - متوكسى - ساليسيليدين - هايدرازين - كاربودايثيوتو - فنانشرولين - اكسى الفانديوم . ولقد تم تعيين المعاملات المغناطيسية لكل من النظامين . ولقد وجد أن مدى تباين الدوران الذى عين للنظامين الأول ( $N = ٢٥ \pm ٥$  . على المحور  $\bar{Z} = Y$ ) والثانى ( $N = ١٧ \pm ٥$  . على المحور  $\bar{Z} = Y$ ) مطابق لنتائج نموذج استوك - انشتاين ، ولعادلة القيم المأذونة (Allowed - Values Equation) ثم تم تحليل اعادة التوجيه الجزيئى لهذين النظامين وذلك بدلالة الاسترخاء الجزيئى فى السوائل ، فوجد أن النظام الثانى يتمتع بصفات لزوجة أعلى من النظام الأول . وكذلك تم تعيين المعاملات المغناطيسية لـ S - ميثيل - N - ساليسيليدين - هايدرازين - كاربودايثيوتو - فنانشرولين - اكسى الفانديوم .



## ABSTRACT

An EPR line width study at 9 GHz was focussed on oxovanadium(IV) systems in the motional narrowing region. The anisotropy of rotation ( $N$ ) and the correlation time ( $\tau_R$ ) were determined. The first system is bis(S-methyl-3-isopropylidenehydrazinecarbodithioato)oxovanadium(IV) in toluene. The second system is S-methyl-N-5-methoxysalicylidenehydrazinecarbodithioatophenanthrolineoxovanadium(IV) in methylene chloride. The magnetic parameters of these two systems were determined.  $N$  obtained for the first system ( $2.5 \pm 0.5$  at an axis  $\bar{Z} = Y$ ) was found to be consistent with the Stokes-Einstein model and the Allowed-Values Equation (AVE) for a monomer in solution with a trans structure.  $N$  obtained for the second system ( $1.7 \pm 0.5$  at an axis  $\bar{Z} = Y$ ) was found to be consistent with the Stokes-Einstein model and the AVE. From the molecular relaxation in liquids analysis, it seems that the solute in the second system is experiencing more stickiness behavior than that in the first system. The magnetic parameters of S-methyl-N-salicylidenehydrazinecarbodithioatophenanthrolineoxovanadium(IV) in toluene were also determined.

CHAPTER ONE

INTRODUCTION

## CHAPTER 1

### INTRODUCTION

#### 1.1 INTRODUCTION

Magnetic resonance studies, at 9 GHz, have been focussed on a model system of  $\text{VO}^{2+}$ , oxovanadium (IV), with sulfur donor ligands [1].

The interest in molecularly characterizing the vanadyl ( $\text{VO}^{2+}$ ) compounds present in heavy crude oil [2], aside from the obvious geochemical interest, resides in the fact that novel removal method of vanadium for process and environmental reasons will ultimately rely on knowing the vanadyl compound composition of these complexes in petroleum matrices.

Three complexes have been studied in this work. The first complex is bis (S-methyl-3-isopropylidenehydrazinecarbodithioato)oxovanadium(IV),  $\text{VO}[(\text{CH}_3)_2\text{C}=\text{NNCSSCH}_3]_2$ , which is proposed to have distorted square pyramidal structure with a cis-configuration, Fig. 1.1, or with a trans configuration, Fig. 1.2, with or without dimerization through sulfur bridges [1].

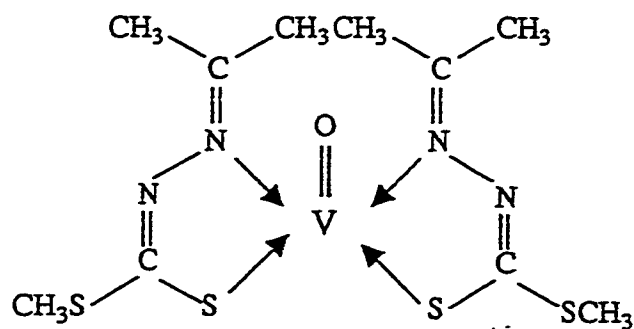


Fig. 1.1 : Cis-VO[(CH<sub>3</sub>)<sub>2</sub>C=NNCSSH<sub>3</sub>]<sub>2</sub>

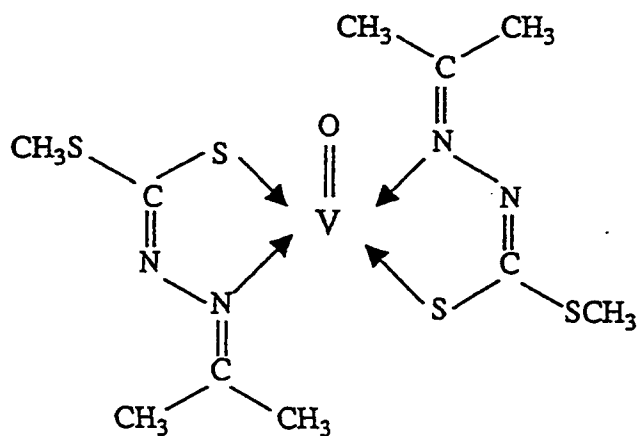


Fig. 1.2 : Trans-VO[(CH<sub>3</sub>)<sub>2</sub>C=NNCSSH<sub>3</sub>]<sub>2</sub>

The second complex is the S-methyl-N-salicylidene-hydrazine carbodithioato-phenanthroline-oxovanadium(IV),  $\text{VO}[\text{Sal SB}](\text{Phen})$ , which is a monomeric octahedral complex, as shown in Fig. 1.3.

The third complex is the S-methyl-N-5-methoxy-salicylidene hydrazine-carbodithioato-phenanthroline-oxovanadium(IV)  $\text{VO}[(5\text{-MeO Sal SB})(\text{Phen})]$ , which has a monomeric octahedral structure, as shown in Fig. 1.4 [1].

The EPR spectrum of each of these vanadyl complexes consists of an eight-line spectrum arising from the interaction of a single unpaired electron ( $S=1/2$ ) with the quenched orbital angular momentum of vanadium nucleus of spin ( $I=7/2$ ).

The goals of this study are (1) to determine the magnetic parameters of these compounds in the rigid limit region, (2) to analyze whether the vanadyl complexes are carrying out anisotropic rotational reorientation in liquids from analysis of the line shape as a function of temperature, and (3) to determine the hydrodynamic radii of the solvated vanadyl complexes in neat solution in order to determine if the compound is cis or trans.

In the first part of this thesis, the magnetic parameters of these three complexes are obtained from the rigid limit and the room temperature spectra according to Wilson and Kivelson's method [3]. These magnetic parameters are necessary for a proper interpretation of

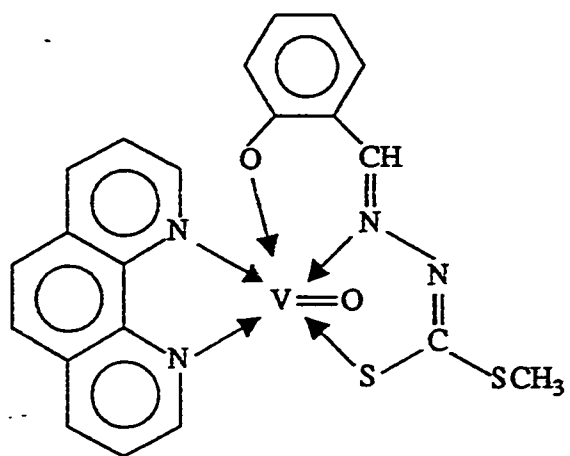


Fig. 1.3 : VO[Sal SB](Phen)

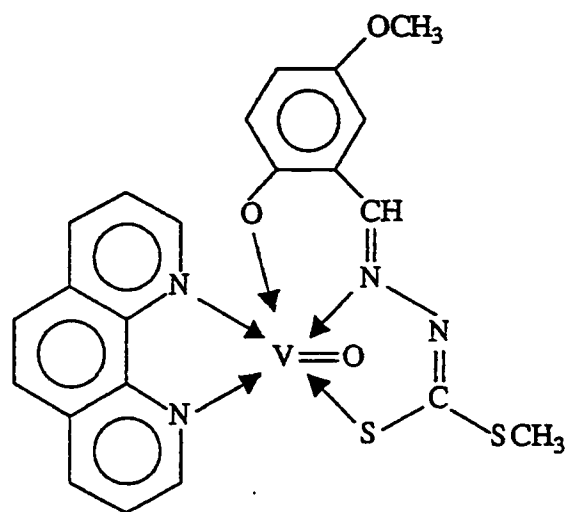


Fig. 1.4 : VO[5-MeO-Sal SB](Phen)

the observed EPR spectra at various temperatures in terms of correlation time ( $\tau_R$ ) and anisotropic rotational diffusion (N).

In the second part, the EPR spectra of  $\text{VO}[(\text{CH}_3)_2\text{C}=\text{NNC}(\text{SCH}_3)_2]$  in toluene and  $\text{VO}[5\text{-MeO Sal SB}](\text{Phen})$  in methylene chloride at various temperatures, in the motional narrowing region, are analyzed to study the anisotropy of molecular rotation (N) defined as the ratio  $R_{\parallel}/R_{\perp}$ , where  $R_{\parallel}$  is the rotational diffusion constant along the molecular principal axis of rotation and  $R_{\perp}$  is the rotational diffusion constant perpendicular to the molecular principal axis of rotation [4,5,6]. Our results are compared with the anisotropy of rotation, N, calculated from Stokes-Einstein model [7] and that calculated from the Allowed-Values Equation (AVE) [8]. This comparison demonstrates the applicability of these narrowing motion region equations to experimentally observable system as well as giving some valuable information about the structure.

From the analysis of the temperature dependent EPR line shapes in the motional-narrowing region the stickiness factor (S) [9,10,11] which is a measure of all non-hard-core interactions, is also determined. The stickiness factor is independent of molecular geometry and is zero in the slip and 1 in the stick limit,  $0 \leq S \leq 1$ . The stickiness factor (S) defined as:

$$S = \frac{\kappa - C_{\text{slip}}^{\text{hyd}}}{1 - C_{\text{slip}}^{\text{hyd}}} \quad (1.1)$$

where  $\kappa$  is a dimensionless anisotropic interaction parameter which measures the coupling of the rotational motions of the probe to the translation modes of the fluid [9,10] and  $C_{\text{slip}}^{\text{hyd}}$  is the empirically determined factor which depends on the nonhydrodynamic character of the friction and on the shape of the molecule.

In the remainder of this chapter a brief account of the magnetic properties of vanadium spin probes, the Kivelson methods of determining the isotropic and anisotropic magnetic parameters [3] and the EPR in the motional narrowing region [4,5,6] is given.

In Chapter 2, we describe the spectrometers used in performing the experiments, and in Chapter 3, the experimental procedures. In Chapter 4, we demonstrate how the magnetic parameters are obtained and how dependence of line widths on temperature is utilized to obtain the anisotropic factor ( $N$ ), and the correlation time ( $\tau_R$ ). These experimental  $N$  values are compared with the theoretical values [7,8].

In Chapter 5, the experimental results and the conclusions are given.



## 1.2 ELECTRON PARAMAGNETIC RESONANCE

Electron Paramagnetic Resonance (EPR), also known as Electron Spin Resonance (ESR), is a technique which records transition between spin levels of molecular unpaired electrons in external magnetic field. EPR spectroscopy [12-14] involves absorption of energy from electromagnetic radiation in the microwave frequency region by a sample placed in an external magnetic field. Absorption is a function of unpaired electrons present in the molecule. A plot of the absorption of the microwave energy versus the external magnetic field gives an EPR spectrum.

EPR has proven to be a powerful technique for spectroscopic study of any system that possesses a net electron spin angular momentum. Typical examples of systems that are amenable to study by EPR include free radicals produced by physical or chemical means in the solid, liquid or gaseous state; biradicals, molecules containing two unpaired electrons at sufficient separation such that unpaired electrons only weakly interact; triplet state molecules, which include ground state triplet molecules as well as triplet states produced by thermal or photochemical excitation; conduction electrons in metals; applications to biochemical and biomedical problems; semiconductors; and most of the transition metal ions.

The spin probe could be a paramagnetic metal ion of the transition or lanthanide series, or a nitroxide radical. One of the popular probes is the vanadyl spin probe. The vanadyl spin probe has paramagnetic

properties due to the existence of an unpaired electron ( $d^1$ -system). A number of factors contribute to the popularity of these spin probes, for example, many vanadyl probes can easily be obtained and purified; they are stable over a wide range of temperatures and do not, therefore, undergo appreciable changes in magnetic parameters with variation in temperature; they are readily soluble in many organic solvents; they have an electron spin of  $1/2$  and its orbital contribution to the magnetic moment is largely quenched, they have only vanadium nuclear moment which contributes to the spectrum and they do not therefore involve any complications found in systems with several nuclear spins [15]. Thus the subsequent theoretical analysis is simplified and the results are easier to interpret than for typical nitroxide spin probes with less symmetry [16]. Also the characteristic eight hyperfine line EPR spectrum of vanadyl complexes provides a more severe testing of any theoretical analysis than a three hyperfine line nitroxide spectrum would provide. In addition, inhomogeneous broadening is usually negligible in the EPR spectra of vanadyl complexes [15].

There are two techniques related to the vanadyl spin probes: the spin labelling and the spin probe techniques [17-19]. Spin labelling is a technique which involves covalent bonding of vanadyl probe to diamagnetic media like liquid crystals. For systems with no inherent paramagnetism, a great advantage is gained by introduction of some versatile probe containing a paramagnetic centre. Line width

measurement of the EPR spectra of covalently bound spin label may give information on the mobility of macromolecules. The spin probe technique is a method whereby different paramagnetic centres are mixed with the diamagnetic host (unbound), and their tumbling behavior during relaxation and transition process in the diamagnetic host is studied. The spectral changes result from restrictions in the motional freedom imposed upon the probe by its microenvironment. The vanadyl spin probe studies have been performed in liquid and frozen media [4-6], petroleum [2], poly(vinyl alcohol)gels [20], liquid crystals, human serotransferrin [21] as well as many other biological systems [22].

EPR methods can be applied to reveal three of the most important types of information: (1) the environment of the vanadyl ion, (2) the nature of ligand types, and (3) the distortion of complexes and association with systems.

### 1.3 SPIN HAMILTONIAN AND DEFINITION OF THE PARAMETERS

The appropriate spin Hamiltonian,  $H_S$ , required to describe the vanadyl paramagnetic systems in general is [18,19]:

$$H_S = B \beta_0 g \cdot S + S \cdot A \cdot I + (\text{electron-electron dipole term}) + \\ + (\text{electron-electron exchange term}) + (\text{nuclear Zeeman term}) \quad (1.2)$$

The first term ( $B \beta_0 g \cdot S$ ) is the electron Zeeman term and the second term ( $S \cdot A \cdot I$ ) is the electron-nuclear hyperfine interaction term; where  $\beta_0$  is electron Bohr magneton,  $B$  is the laboratory magnetic field,  $g$  the electron  $g$ -value tensor,  $S$  is the electron spin angular momentum operator,  $A$  is the electron-nuclear hyperfine tensor, and  $I$  is the nuclear spin angular momentum operator. The nuclear Zeeman term is not important in most work [23] and will be omitted. For clarity small second order effects are not discussed here. The electron-electron dipole and exchange terms are significant only when very high concentration [24] and single crystals studies [25] are considered.

#### 1.3.1 EPR Spectra in Solution

The EPR spectra of these vanadyl complexes in liquid solutions can be described by the isotropic electron Zeeman and electron-nuclear hyperfine interactions included in the spin Hamiltonian [3,26]:

$$H_s = \beta_o gS B + h I \underline{A} S \quad (1.3)$$

where  $\beta_o$  is the Bohr magneton,  $S$  is the electron spin operator,  $I$  is the nuclear spin operator,  $B$  is the applied magnetic field,  $g$  is the  $g$ -value tensor and  $\underline{A}$  is the hyperfine interaction tensor of the  $^{51}\text{V}$  nucleus [26].

The allowed transitions, when a microwave field at frequency  $\omega_o$  is applied, occur at the field  $B$  which satisfies the resonance condition [3,26]

$$\omega_o = g_o \beta_o B/h + A_o M + \frac{1}{2} A_o^2 \left[ \frac{I(I+1)-M^2}{g_o \beta_o B/h} \right] \quad (1.4)$$

where  $\omega_o$  is the microwave frequency in radians per second,  $h$  is the Planck's constant divided by  $2\pi$ ,  $I = 7/2$ ,  $M$  is the nuclear spin magnetic moment,  $B$  is the resonant value of the magnetic field corresponding to  $M$ ,  $A_o$  is the isotropic hyperfine constant in radians per second:

$$A_o = \frac{1}{3} (A_x + A_y + A_z), \quad (1.5)$$

and  $g_o$  is the isotropic  $g$ -factor :

$$g_o = \frac{1}{3} (g_x + g_y + g_z), \quad (1.6)$$

where X, Y and Z refer to the molecule fixed coordinates, and it has been assumed that g and A can be simultaneously diagonalized. The contact hyperfine constant  $A_0$  can be obtained to second order by taking the difference of  $B_M$  for line M and  $B_{-M}$  for line -M:

$$A_0 = -g_0 \beta_0 (B_M - B_{-M})/2Mh \quad (1.7)$$

Furthermore,

$$g_0 - g_s = g_s \left\{ |B_s - \frac{1}{2}(B_M + B_{-M})| / \frac{1}{2}(B_M + B_{-M}) \right\} \\ - 2A_0^2 h^2 |I(I+1) - M^2| / g_s \beta_0^2 (B_M + B_{-M})^2, \quad (1.8)$$

where  $g_s$  and  $B_s$  are the isotropic g-value and the resonant value of the magnetic field (in Gauss), respectively for standard of known g-value. For our system, the standard used is diphenylpicrylhydrazyl (DPPH), for which  $g_s$  value is 2.0037.

The first term in equations (1.2) and (1.3), the electron Zeeman term, represents the large interaction of the electron spin with the laboratory magnetic field. This term yields the useful relation:

$$h\nu = g_0 \beta_0 B \quad (1.9)$$

where h is Planck's constant and  $\nu$  is the microwave frequency of the EPR spectrometer.

Equation (1.9) may be reduced to [27]:

$$\nu \text{ (in GHz)} = 2.80247 \frac{g_0}{g_e} B \text{ (in kG)} \quad (1.10)$$

where  $g_e$  is the  $g$ -value for free electron.

For vanadyl complexes equation (1.10) can be further reduced to

$$\nu \text{ (in GHz)} = 2.847 B \text{ (in kG)} \quad (1.11)$$

This relation serves as a useful conversion factor. Most EPR spectrometers operate at  $\nu = 9.5$  GHz (X-band), and thus  $B = 3.3$  kG. Some spectrometers operate at higher frequencies, for example at  $\nu = 35$  GHz (Q-band), where  $B = 12.3$  kG. There is very little difference between the spectra recorded at the two frequencies when the paramagnetic centres are rapidly tumbling.

The unpaired electron responsible for the EPR spectrum is confined largely to the vanadyl centre. This unpaired electron interacts with the nuclear spin of  $^{51}\text{V}$  ( $I = 7/2$ ), the result is  $(2I + 1)$  or 8 lines separated by a coupling constant with different intensities. This electron nuclear interaction is represented by the second term in equation (1.2).

It is apparent from the variation in the intensities of the lines that the line widths of the different hyperfine components are not equal and depend on the  $^{51}\text{V}$  nuclear spin quantum number [3,26]. This line

width variation indicates that the anisotropic hyperfine and Zeeman interactions are not completely averaged out by the tumbling of the molecules in the liquid, and they contribute significantly to the lines widths.

The relationships of the important  $A_0$  and  $g_0$  parameters are shown in Fig. 1.5 along with the lines widths ( $\Delta H$ ) and the peak heights ( $h$ ) in a first derivative representation of the absorption curve. The EPR spectrum can be displayed in various ways, namely the absorption curve, the integral of the absorption curve, first and second derivatives of the absorption curve. The first derivative is the most common representation in the literature. The spectra can also be recorded with the opposite phase from that in Fig. 1.5 (producing an upside-down effect). The choice of the phase and scan direction results in four possible permutations of the same spectrum. Although all the four permutations can be found in the spin labelling and the spin probing literature, the presentation most consistent with current trends in spectroscopy involves positive phase and increasing B from left to right. All spectra presented in this thesis follow this convention.



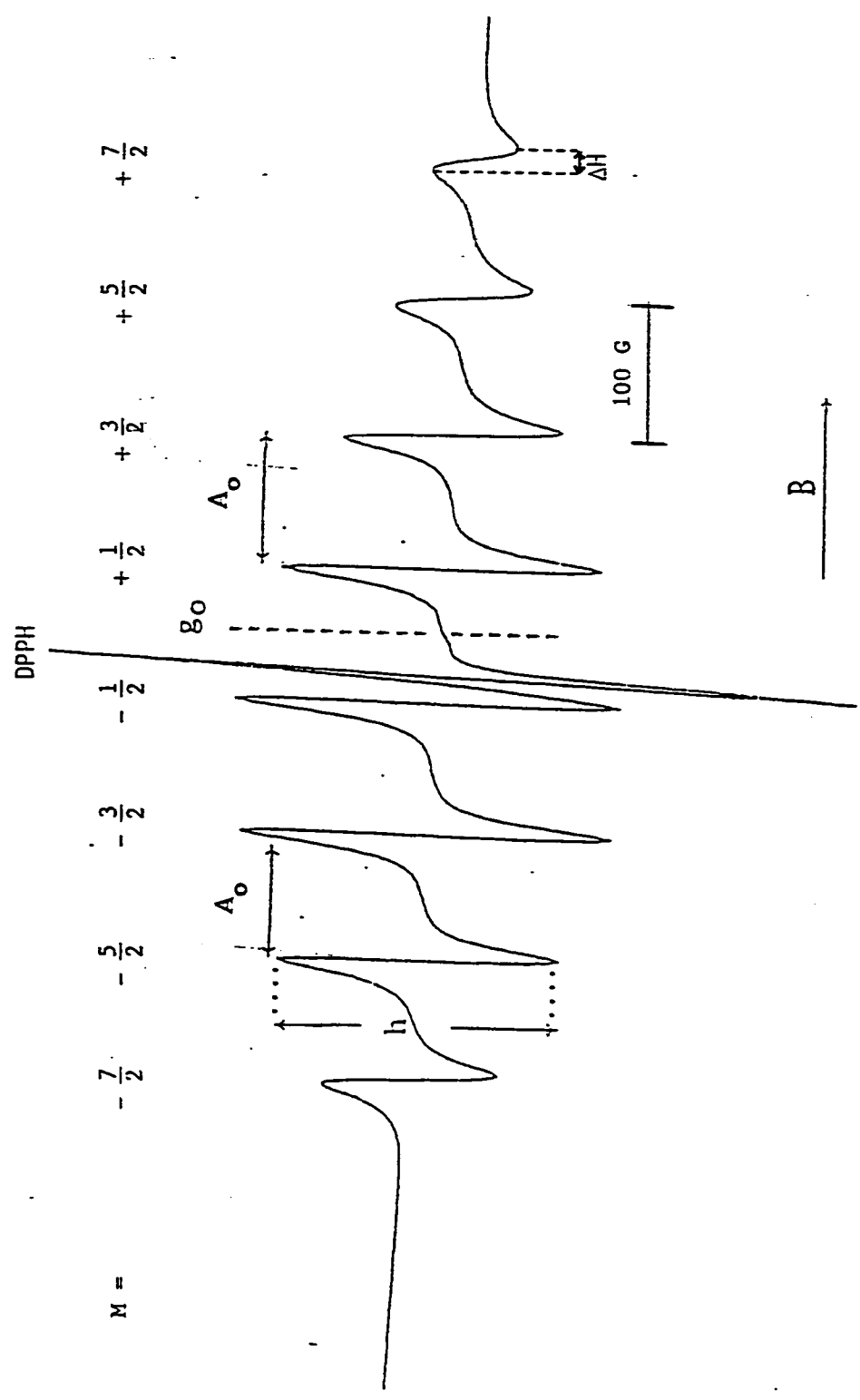


Fig. 1.5: A Typical X-band Spectrum of Oxovanadium (IV) in Solution at Room Temperature.

### 1.3.2 EPR Spectra in the Absence of Molecular Motions

#### 1.3.2.1 Anisotropic Effects

The glass spectrum of vanadyl probes can be described in terms of the Zeeman and nuclear-electronic hyperfine interactions by the spin Hamiltonian [3,19,28]:

$$H_s = \beta_o (g_x B_x S_x + g_y B_y S_y + g_z B_z S_z) + A_x S_x I_x + A_y S_y I_y + A_z S_z I_z \quad (1.12)$$

a special case of Eq. (1.2). Both  $g$  and  $A$  depend on the orientation of the magnetic field in terms of molecular coordinates and the direction of  $B$ . The extremes in  $g$  and  $A$  lie along the principal  $X$ ,  $Y$  and  $Z$  axes. The  $Z$ -axis is along  $V-O$  bond.

The glass EPR spectrum of a typical  $VO^{2+}$  (at 77 K) is illustrated in Fig. 1.6. This glass spectrum of vanadyl complexes is governed by [3]:

$$\omega_o = g\beta_o B_M/\hbar + AM + \frac{(A_x^2 + A_y^2)(A_z^2 + A^2)}{8A^2} \frac{|I(I+1) - M^2|}{g\beta_o B_M/\hbar} \quad (1.13)$$

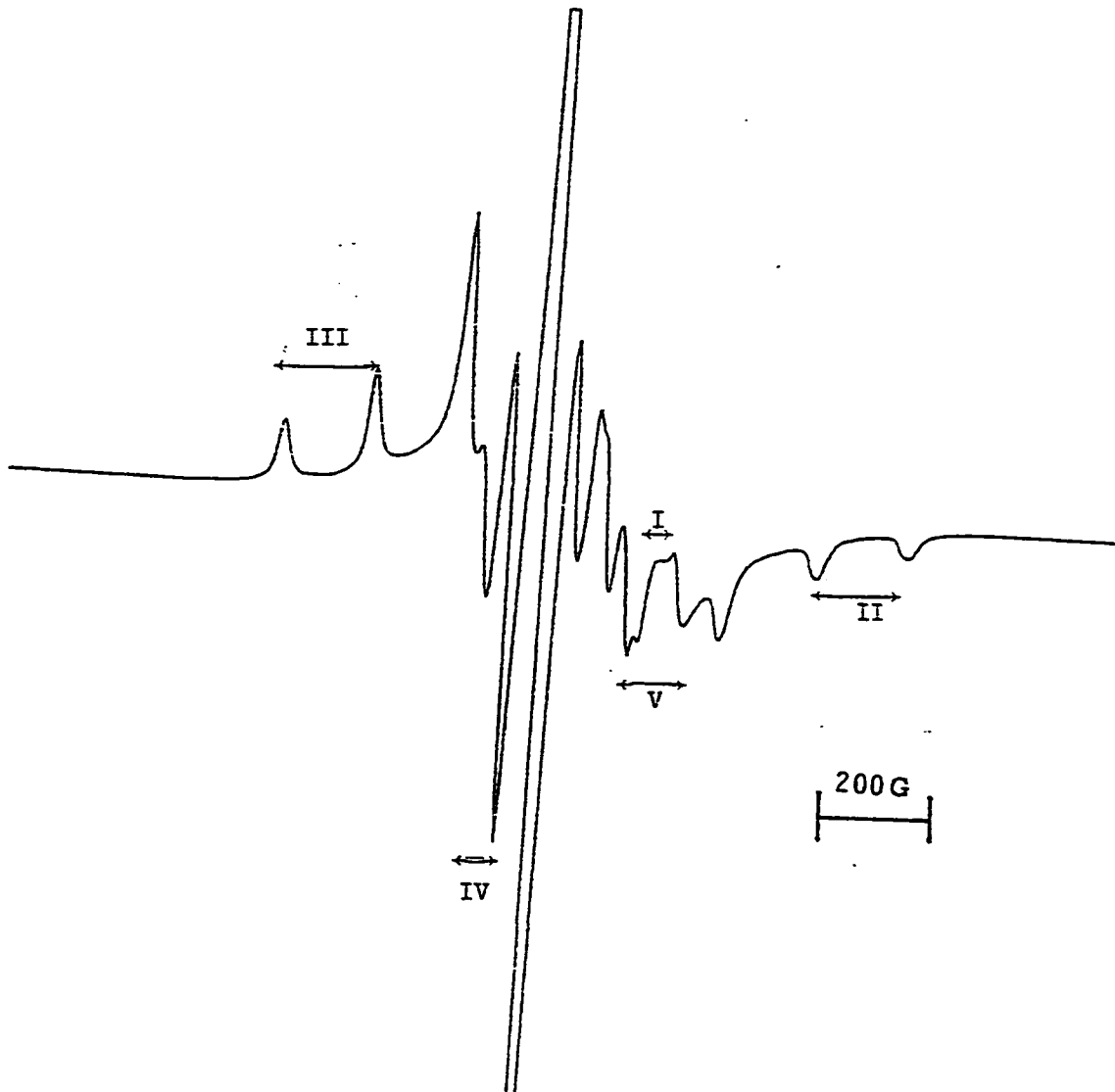


Fig. 1.6: A Typical X-band Spectrum of Oxovanadium (IV) at 77 K.

where

$$g = (g_z^2 \cos^2 \theta + g_x^2 \sin^2 \theta \cos^2 \varphi + g_y^2 \sin^2 \theta \sin^2 \varphi)^{\frac{1}{2}},$$

$$gA = (A_z^2 g_z^2 \cos^2 \theta + A_x^2 g_x^2 \sin^2 \theta \cos^2 \varphi + A_y^2 g_y^2 \sin^2 \theta \sin^2 \varphi)^{\frac{1}{2}}$$

$\theta$  is the angle between B and unique molecular axes, presumably the vanadyl VO axis, and  $\varphi$  is the azimuthal angle. Note that the line for which  $\theta = 0$  gives rise to the spectrum corresponding to  $g_z$  and  $A_z$  in Fig. 1.6, while those for which  $\theta = \varphi/2$ ,  $\varphi = 0$  and  $\pi/2$  give rise to the "doubled spectra" corresponding to  $(g_x, A_x)$  and  $(g_y, A_y)$  in Fig. 1.6.

The anisotropic tensors can be determined from rigid limit spectra, Fig. 1.6, as Wilson and Kivelson have done for vanadyl acetylacetonate (VOAA) [3]. If we consider spacings I, II, III, IV and V in Fig. 1.6. then

$$A_z = \frac{II + III}{2} \tag{1.14}$$

$$A_x + A_y = IV + V \tag{1.15}$$

$$I = \beta_0 B 2\delta_g/h + 4c(7/2) \quad (1.16)$$

where

$$\delta_g = \frac{1}{2}(g_x - g_y) \quad (1.17)$$

$$c = \frac{1}{4}(A_x - A_y) \quad (1.18)$$

Although the values of  $g_x$ ,  $g_y$ ,  $g_z$  and  $A_x$ ,  $A_y$ ,  $A_z$  obtained from the glassy spectrum are compatible with the isotropic values obtained from the liquid spectrum, the most accurate determinations of the magnetic parameters are obtained by measuring  $g_0$  and  $A_0$  from the liquid spectrum;  $g_z$ ,  $g_x - g_y$ ,  $A_z$  and  $A_x - A_y$  from the glass spectrum, and  $g_x$ ,  $g_y$ ,  $A_x$  and  $A_y$  from this data and equations 1.5 and 1.6 [3].

### 1.3.2.2 The Effects of Rotational Motion on EPR Spectra

The shape of an EPR spectrum is markedly dependent upon the rotational mobility of the paramagnetic spin probe. For example, in a nonviscous solvent nearly all vanadyl probes exhibit eight sharp lines. The rapid isotropic tumbling motion averages away all anisotropic effects discussed above and, therefore sharp lines are obtained. If the rotational motion is slowed down by increasing the solvent viscosity, averaging is incomplete. The result is unequal broadening of the eight derivative lines. Molecular motion is not necessarily isotropic. Preferential motion about one axis is likely to occur for any asymmetric spin probe, but the effects are particularly evident when surrounding medium is anisotropic. The EPR spectrum is very sensitive to the probe mobility. The best way to make use of this sensitivity is to describe the motion quantitatively in terms of the shape of the spectrum.

As discussed above, both the anisotropic hyperfine electron-nuclear interaction and the anisotropic spin-orbit interaction in a spin probe depend on the mutual orientation of the external magnetic field and of  $\pi$ -orbital of the unpaired electron. Rotations of the probe modulate these interactions, leading to fluctuations in local magnetic fields and changes of the EPR line widths. Rotational motion is characterized by correlation time ( $\tau_R$ ) which determines the effective frequency of

rotation, ( $f_{\text{eff}}$  in Hz):  $f_{\text{eff}} = (2\pi\tau_R)^{-1}$ . The principal  $g$  and  $A$  values are related to the isotropic  $g_0$  and  $A_0$  values through equations (1.5) and (1.6).

The anisotropy of  $g$  and  $A$  tensors is applied in dynamic spin probe studies to get information about the motional state of the probe. Between the two limits of very rapid motion and a rigid glass, the spectra are quite complex. This complexity provides much of the information that can be obtained about molecular motion using spin-probe techniques.

#### 1.4 THE CORRELATION TIME GROUP

The correlation time data of vanadyl complexes is usually divided into three groups:

Rapid rotations :  $10^{-11} - 10^{-9}$  sec.

Slow rotations :  $10^{-9} - 10^{-6}$  sec.

Very slow rotations :  $10^{-6} - 10^{-3}$  sec.

The limits of these regions are essentially determined by the anisotropy of the magnetic interactions occurring in the probes.

## 1.5 MOLECULAR TUMBLING

The spin Hamiltonian can be divided into:

$$H = H_0 + H_1(\Omega) + \varepsilon(t) \quad (1.19)$$

where

$$H_0 = \beta_0 g_0 B S_z + A_0 I \cdot S \quad (1.20)$$

where  $S_z$  is the electron spin along the Z-axis,  $S$  and  $I$  are the electron and the nuclear spin operator,  $B$  is the laboratory magnetic field, and  $\beta_0$  is electron Bohr magneton, and

$$H_1 = \beta_0 B \cdot g S + I \cdot \underline{A} \cdot S \quad (1.21)$$

where  $g$  and  $\underline{A}$  contain the anisotropic components of the electron  $g$ -tensor and electron-nuclear dipole hyperfine tensor after the isotropic components  $g_0$  and  $A_0$  have been subtracted. These tensors are defined in terms of molecular fixed axis whose orientation varies with time with respect to the laboratory magnetic field due to molecular motion. Thus the time dependence of  $H_1$  is modulated by the reorientational motion of the molecule ( $\Omega$ ), and

$$H_1(t) = \frac{1}{2} h \gamma_e B [S_x \exp(-i\omega t) + S_x \exp(i\omega t)] \quad (1.22)$$



where

$$S_+ = S_x + iS_y$$

is the raising operator,

$$S_- = S_x - iS_y$$

is the lowering operator,  $\gamma_e$  is the magnetogyric ratio of a free electron

and  $\omega$  is the microwave frequency.

$\varepsilon(t)$  gives the interaction of the spin with the microwave radiation field which must be included in the Hamiltonian if the saturation effects are to be considered. Since saturation effects are known to be negligible for experimental spectra discussed in this work, only terms linear in  $\varepsilon(t)$  must be considered [28].

The term "fast" and "slow" refers to the randomly fluctuating part  $H_1(t)$  of the spin Hamiltonian (where  $H_1(t)$  has a time averaged value zero) in relation to a correlation time  $\tau_R$  which characterizes the underlying stochastic process. Fast motional theories are applicable if  $|H_1(t)|\tau_R \ll 1$  (where  $H_1(t)$  is expressed in frequency units). On the other hand, the rigid limit is attained when  $|H_1(t)|\tau_R \gg 1$ .

Since the slow and the very slow rotations lie outside the scope of this work, only the fast tumbling rotation will be discussed.

## 1.6 FAST TUMBLING

It is convenient at this point to define a line width parameter  $T_2$ . If the peak to peak width is  $\Delta H$  (in gauss.), then  $T_2^{-1} = \Delta H$ . In general, the dependence of  $T_2$  upon  $M$ , the component of the nuclear spin along the direction of the applied magnetic field is given by:

$$T_2^{-1}(M) = A + BM + CM^2 + X \quad (1.23)$$

where  $A$ ,  $B$  and  $C$  depend on the magnetic tensors and  $X$  takes into account other possible broadening mechanisms. The line width contributions can be calculated with the Redfield relaxation matrix theory as applied by Freed and Fraenkel [29,30] or with the theory of Kubo and Tomita as applied by Kivelson [31].

In order to determine the anisotropy of rotation ( $N$ ) and the axis of rotation, the motional narrowing analysis of Freed et al [4-6] has been used and Eq. (5) in ref. [6] has been used. In practice,  $\tau_R$  is obtained from  $B$  and  $C$  because of the uncertainty in  $A$  [24]. The theoretical expressions for  $B$  and  $C$  coefficients [4,5,32] will be discussed in details in chapter 4.

For isotropic Brownian diffusion  $\tau_R = (6R)^{-1}$  where  $R$  is the rotational diffusion coefficient. For the eight lines spectrum for

vanadyl probe, Eq. (1.23) will give rise to three experimentally determined unknowns, A, B and C. Since the line width coefficients B and C are functions of  $\tau_R$  values, in the case of two values of  $\tau_R$  value not agreeing, the assumption of anisotropic rotation must be suspected. Fortunately, this restriction has been resolved by Freed and his co-workers [5,33]. The quadratic dependence of  $T_2^{-1}$  on M given in Eq. (1.23) is retained, but the motion is described by a rotational tensor R. This is often axially symmetric and is defined by two components  $R_{\parallel}$  and  $R_{\perp}$  where  $R_{\parallel}$  is the rotational diffusion constant along the principal axis of rotation, and  $R_{\perp}$  is the rotational diffusion constant perpendicular to the principal axis of rotation. The anisotropy of rotation (N) is defined as the ratio of  $\frac{R_{\parallel}}{R_{\perp}}$ . Two related correlation times  $\tau(0)$  and  $\tau(2)$  are given by:

$$\tau(0) = (6 R_{\perp})^{-1} \quad (1.24)$$

$$\tau(2) = (2 R_{\perp} + 4 R_{\parallel})^{-1} \quad (1.25)$$

Reference should be made to the original literature [5,33] and the more recent work [34] for details of this analysis.

## CHAPTER TWO

### APPARATUS

## CHARTER 2

### APPARATUS

#### 2.1 INTRODUCTION

The instruments used to record EPR spectra are as follows:

- (1) Varian E-109 EPR spectrometer, Varian E-935 Data Acquisition system which also employs the HP-9835 computer for data processing.
- (2) Bruker ER-200D-SRC spectrometer, Bruker ER140 Data system which is interfaced with 96 MB Hard disk from Control Data Corporation.
- (3) Pope Scientific Inc. vacuum system for degassing the sample tubes.

#### 2.2 VARIAN E-109 EPR SPECTROMETER

##### 2.2.1 General Description

The individual units of the E-109 spectrometer are:

An electronic (operator's) console, a microwave bridge, a sample cavity with connecting waveguide, a magnet, and a magnet power supply. The system is completely solid state in design with the exception of reflux klystron tube in the microwave bridge and the

cathode ray tube in the oscilloscope.

The basic electronic console contains the following modules and assemblies:

- (1) The E-203B Magnetic Field Controller provides direct control and regulation of the magnetic field in the magnetic air gap .
- (2) The E-207 High Frequency Module provides magnetic field modulation frequencies of 25 kHz and 100 kHz .
- (3) The E-200 oscilloscope displays the EPR signals for visual observation and the klystron power mode for spectrometer tuning.
- (4) The E-080B digital drive recorder graphically displays the EPR spectrum as a function of magnetic field or time.

The E-102 microwave bridge provides controlled 9.5 GHz microwave frequency to the cavity and detection of EPR signals. The absorption reference arm design permits operation at microwave power levels to one microwatt .

The E-231 series sample cavity is a multipurpose rectangular cavity with an 11 mm sample access. The cavity is designed to permit up to 40 G peak-to-peak field modulation at the sample.

The magnet used is 9-inch in size with the magnet power supply providing the d.c. power to the magnet. The magnet and microwave

bridge are water cooled and the chilled water supplied by a mechanically refrigerated closed circuit water chiller.

To measure the field value up to 6 significant figures a Varian E-500 NMR gauss meter is used. Similarly, to get the accurate value of the frequency, HP model 5342A microwave frequency counter is used.

## **2.2.2 Data Acquisition**

### **2.2.2.1 Introduction**

The E-935 Data Acquisition system consists of the following four units:

HP 9835 computer

E-935 Data Acquisition System

HP 1350A Graphics Translator

HP 1311A CRT Display

With the use of this computer, one can store the experimental data on a cartridge and later retrieve the data for various analyses, like plotting, manipulation of data, and calculations like g-factor, etc. The data collection becomes fast and efficient with the use of computer.

#### **2.2.2.2 E-935 System Software**

The software ( provided by Varian Instrument Co. ) is divided into four functional modules. Only one of these modules can be present in the memory of the HP 9835 computer at a time. The four functions are calculations, manipulations, plotting and scanning.

#### **2.2.2.3 Magnet Scan**

EPR data may be acquired while the large magnet is swept. Magnet scan acquires EPR spectra containing 512, 1024, 2048 or 4096 data points, performs multiscan averaging, and continuously displays the current results on the display unit. Scan times may be in the range of 4-17,000 seconds.

#### **2.2.2.4 Data File Capability**

An EPR spectrum may be stored as a data file on a tape cartridge along with a file header containing descriptions of the sample. Experiment and the instrumental settings like field, frequency, power, modulation frequency modulation amplitude, number of scans, scan time, time constant, microwave power, etc. are stored in the file.

Such a data file may be retrieved from a tape cartridge, loaded into computer memory, and subsequently displayed on the display unit.



Additional operations can be done on the display with the manipulation module. Also a printed catalogue of the files on a given tape cartridge may be obtained. The displayed spectrum can be immediately plotted.

#### 2.2.2.5 Data Manipulation

With the help of the manipulation module, the following manipulations of EPR spectra may be performed using the interactive capabilities of the display unit and key board:

- (1) Base line adjustment of a spectrum.
- (2) Combination of two spectra.
- (3) Detection of erroneous feature from a spectrum.
- (4) Differentiation of a spectrum.
- (5) Digital filtration of a spectrum.
- (6) Double integration of a spectrum.
- (7) X, Y axes scale and shift modifications.
- (8) Editing of the file header and recording the spectrum after editing.

#### **2.2.2.6 Tape Cartridge and File System**

The tape cartridge serves two main purposes. First, the system tape cartridge contains all of the programs required for proper system operation. The second purpose is to provide for long or short term off-line storage of EPR data sets.

Before use all tapes must be initialized as per given procedures. An initialized tape is divided into a total of 852 records of 256 bytes per record. There are two tracks per tape. Records 0-425 on the first track, while records 426-851 are on the second track. All information stored on a tape is saved in the form of files. All data are contained in a particular file name. To retrieve any data later, a file name must be read to the computer.

### **2.3 BRUKER ER-200D-SRC**

#### **2.3.1 General Description**

The ER-200D-SRC is an electronic equipment which can be combined in various ways to make up a number of EPR spectrometers with different capabilities to suit the requirements of the users in different scientific fields. The main assemblies of ER200D-SRC are: a magnet, a microwave cavity and a safety box, a magnet power supply unit (PSU), a microwave bridge and a console. The components, time base unit (ER-001) provides the central timing control for data accumulation, a

signal channel (ER-022) is a signal enhancement and processing unit and a field controller (ER-031M) permits the operator to establish the d.c. magnetic field and the range for the magnetic field sweep width. All these are mounted in the console, which incorporates with power supply units and interconnections for these units. The chart recorder is also mounted in the console. The cavity is supported between the poles of the magnet by a wave guide which is connected to the microwave bridge. The microwave bridge and the magnet are water cooled and the chilled water supplied by a mechanically refrigerated close circuit water chiller. Variable temperature studies were done by using a Bruker ER411 VT variable temperature controller.

### 2.3.2 The Microwave Bridge

The microwave excitation and detection system in conjugation with the associated control electronics for the microwave components, is referred to as microwave bridge. There are four microwave bridges in the range covering 1 to 40 GHz. The microwave radiation is derived from a coherent radiation source such as a klystron or Gunn diode. The incident power is altered by the Rotary vane microwave attenuator and directed to the sample by a unidirectional microwave circulator. The circulator directs power from the source to the sample cavity.

### 2.3.3 The Microwave Probe (Cavity)

The microwave probe, referred to as cavity, serves to contain the sample in the magnet air gap. For each microwave bridge in the range covering 1 to 40 GHz has a separate cavity. Each cavity is supplied with "matching box". Thus the change of a microwave bridge needs changing of proper matching box. The cavity which was used along with the 9 GHz microwave bridge is ER-4102-ST.

### 2.3.4 Data System (ER140)

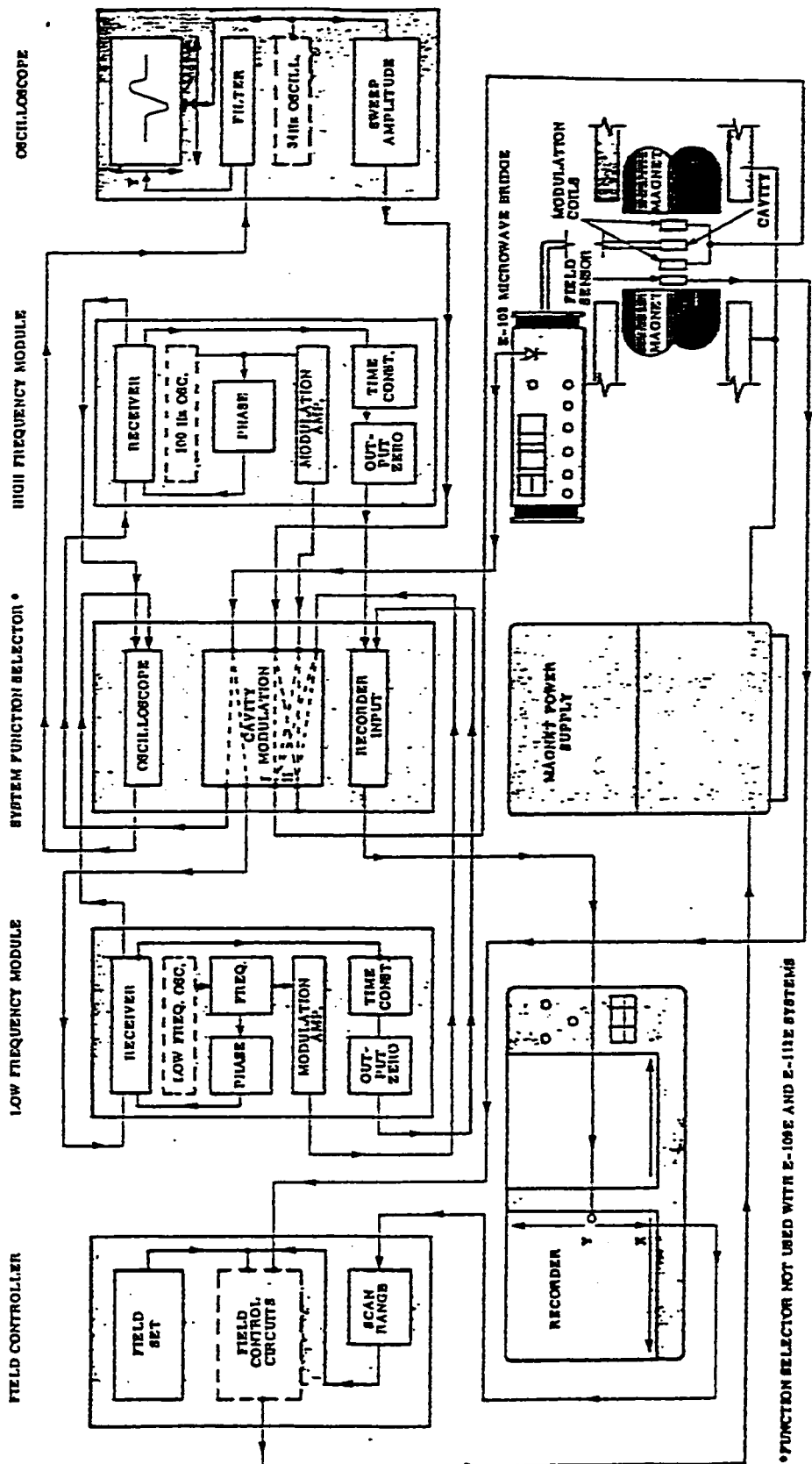
The Bruker ER140 data system, consists of a silent 700 electronic data terminal, a graphic display processor, Aspect controller ER144C, a floppy diskette and a 96 Megabyte hard disk storage.

The spectra are stored in the hard disk which takes hardly a second for recording. Later on while analyzing the spectrum also it could be retrieved in less than one second.

The advantage of Bruker data system which includes the Aspect controller ER144C is, simultaneously three spectra can be displayed. For example one channel could be used for scanning and the other channels for other manipulative works.

#### 2.4. The BASIC EPR SPECTROMETER (FUNCTIONAL DESCRIPTION)

The EPR spectrometer is designed to induce and observe transitions among magnetic dipole moment eigenstates. The EPR signal is observed when the frequency of the electromagnetic field satisfies the resonance condition,  $h\nu = \gamma B$ , where  $h$  is Planck's constant,  $\nu$  is the excitation frequency,  $\gamma$  is electron gyromagnetic ratio and  $B$  represents the total magnetic field strength at the electron including all intrinsic and applied fields. In principle, the EPR spectrum could be observed by monitoring the power observed as a function of the excitation frequency. In this, since EPR is analogous to other spectroscopic techniques performed with radiation throughout the electromagnetic spectrum. However, the ability to modify the eigenvalue spectrum by an applied (external) magnetic field serves to distinguish magnetic resonance from spectroscopy which does not observe magnetic dipole transitions. The functional relationship of the Varian E-109 EPR spectrometer units is illustrated in the block diagram (Fig.2.1). The functional block diagram of the basic ER-200D-SRC spectrometer is shown in Fig.2.2.



\*FUNCTION SELECTOR NOT USED WITH E-109E AND E-113E SYSTEMS

Fig. 2.1 : Functional Block Diagram of Varian E-109 EPR Spectrometer.

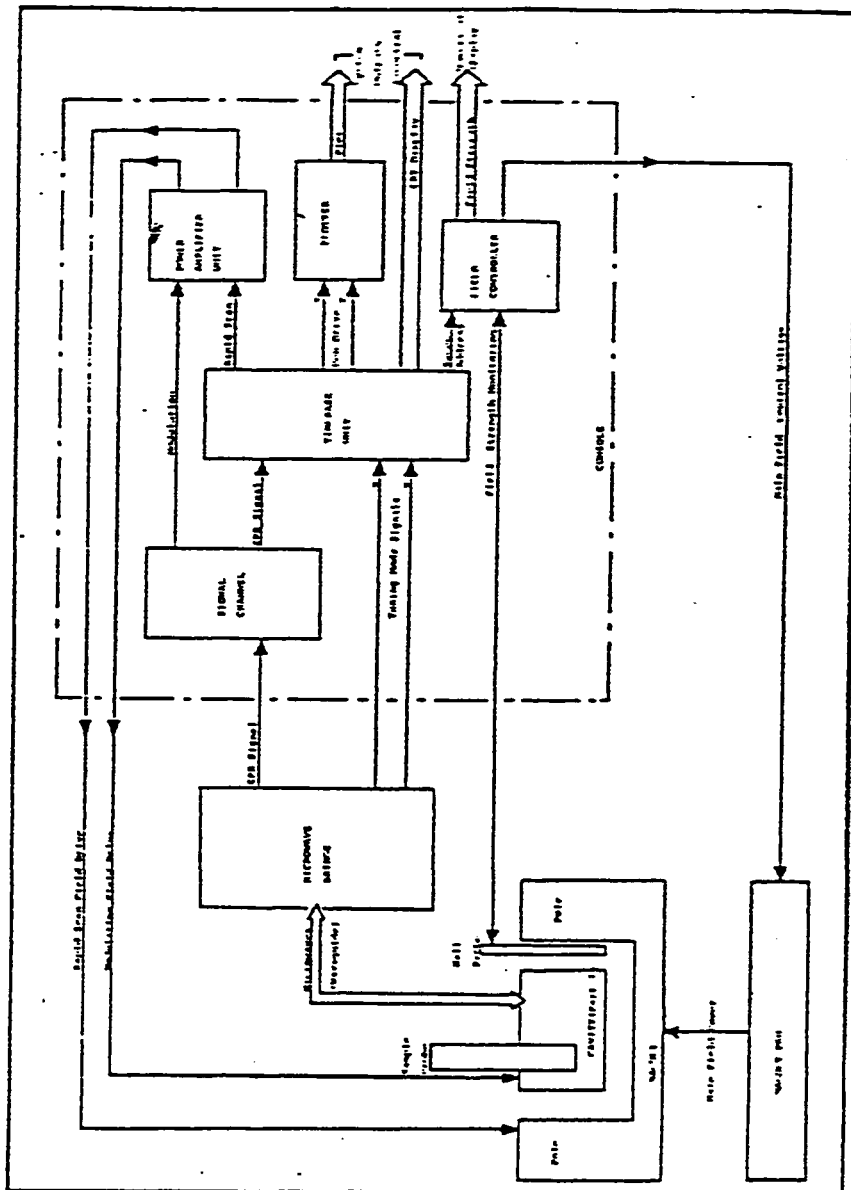


Fig. 2.2 : Functional Block Diagram of ER-200-SRC Spectrometer.

## 2.5 VACUUM SYSTEM

For meaningful EPR line width studies, the sample should be evacuated in order to get rid of oxygen present in the air which is paramagnetic and can interfere with the line width measurements from the paramagnetic sample of interest.

A normal system manufactured by Pope Scientific Inc. was used with slight modifications to suit our needs. One of the modifications is a QUICK FIT arrangement to insert and remove the sample easily. Also, to measure the vacuum readily, we used a digital vacuum gauge manufactured by Granville-Phillips.

Vacuum could be easily reached as low as 1 mTorr and most of the samples were sealed when the vacuum was of that order.



## CHAPTER THREE

### PROCEDURE

## CHAPTER 3

### PROCEDURE

#### 3.1 SAMPLE PREPARATION

##### 3.1.1 $\text{VO}[(\text{CH}_3)_2\text{C}=\text{NNCSSCH}_3]_2$

$\text{VO}[(\text{CH}_3)_2\text{C}=\text{NNCSSCH}_3]_2$  was obtained through private communications [35]. The synthesis was carried out following the procedure outlined in reference [ 1 ].

Samples in the concentration range  $(5 \pm 2)10^{-4}$  M were prepared in toluene (spectroscopic grade purchased from Merck) without further purification. The sample of the above concentration was dripped inside a 2 mm ID pyrex sample tube until the length comes to be one inch, with the help of a very narrow mouthed dropper.

Before degassing a sample, it must be ensured that the sample inside is of right concentration. The method adopted to check the concentration of the sample is the following. The undegassed sample was kept in the cavity of the ESR machine under the following conditions:

Receiver gain                    =  $1.25 \times 10^3$   
Modulation Amplitude         = 0.04 G.  
Microwave power                = 2.0 mW

The above parameters determine the intensity of the peak, and, therefore, under these conditions the intensity of the peak should be within the size of the plotter.

In order to seal the sample tube quickly, one must put on the vacuum line at least one hour before degassing the sample to get good vacuum. The sample is degassed by freeze-pump-thaw procedure which is repeated several times for better degassing.

While sealing the sample, the following precautions are to be taken:

- (1) The length of the sample inside the sample tube must be well immersed inside liquid nitrogen, so that the heat of the torch does not reach the sample.
- (2) The sealing must be done just one to two centimeters above the surface of the sample.
- (3) The length of the sample inside the sample tube must be at least one inch.

Since the sample tube is thin and under pressure, it must be removed very carefully from the vacuum system. 3.1.2

#### VO[Sal SB](Phen)

VO[Sal SB](Phen) complex was obtained through private communications [35]. The synthesis was carried out following the procedure outlined in reference [1].

Samples in the concentration range  $(5 \pm 3)10^{-4}$  M were prepared in toluene (spectroscopic grade purchased from Merck) without further purification.

Sample introduction into the sample tube having 2 mm inside-diameter sample tube, concentration check up, degassing and sealing were carried out in the same way as described for VO[(CH<sub>3</sub>)<sub>2</sub>C=NNCSSCH<sub>3</sub>]<sub>2</sub>.

#### 3.1.3 VO[5-MeO Sal SB](Phen)

VO[5-MeO Sal SB](Phen) was obtained through private communications [35]. The synthesis was carried out following the procedure outlined in reference [1].

Samples in the concentration range  $(5 \pm 3)10^{-4}$  M were prepared in methylene chloride (spectroscopic grade purchased from Merck) without further purification.

Sample introduction to the sample tube, concentration check up, degassing and sealing were carried out in the same way as described for  $\text{VO}(\text{CH}_3)_2\text{C}=\text{NNC}(\text{SCH}_3)_2$ .

## 3.2 DATA COLLECTION

### 3.2.1 EPR Spectrometer Operation

Following is a brief description of how to operate the EPR spectrometer:

- (i) Put on the chiller water for circulation.
- (ii) Turn the console power on and bring the field set slowly to the central field value ( $\cong 3300 - 3400$  G), through the zero value.
- (iii) In the microwave bridge bring the STANDBY setting to TUNE position, while keeping the microwave power around 40 dB.
- (iv) Adjust the iris and turn on the frequency counter.
- (v) While doing variable temperature studies ensure enough purging as well as heat exchanging  $N_2$  gas supply is available and liquid  $N_2$  at the heat exchanger flask is filled fully. Heating element must be properly connected.

### 3.2.2 Spectra Recording

As a general case, insert the sample tube into the cavity; the sample length must be at the active region of the cavity. This could be adjusted with the collars provided. Proper tuning procedure should be followed on the microwave bridge.

Keep the field set at 3300 G, scan range of 1000 G for room temperature spectra. Scan range of 2000 G is used for taking the rigid limit spectra.

For very good line shape analysis, the spectra taken must be free from artifact broadening due to the wrong selection of spectrometer parameters like scan speed, time constant, microwave power, modulation amplitude, etc.

To get the right signal, first increase the modulation amplitude until no peak distortion or line width increase is noticed. This value of modulation amplitude could be used for the experiments subsequently. Second, increase the microwave power until the saturation of the peak occurs.

Time constant setting as thumb rule must be increased one hundred times if the receiver gain is increased ten times. Similarly, scan time must be at least 10 times the value of the time constant.

Once the right spectra are plotted, then they are stored to the tape in the case of Varian Spectrometer or to the hard disk in Bruker. These spectra can be displayed on the screen and analyzed.

For variable temperature experiments, the temperature controlling unit is set at the required temperature and enough time is given for the temperature to become constant. Enough  $N_2$  gas made sure to flow

for heat exchange during high temperature studies. For low temperature study, the heat exchanger is immersed in liquid N<sub>2</sub> and the cavity is purged with nitrogen gas. The 77K spectra are taken without having to use the variable temperature unit. Liquid nitrogen dewar should be filled with liquid nitrogen. To avoid bumping and bubbling, put in a long sheet of filter paper, the filter paper should be kept away from the active region of the cavity. The spectra were taken while purging the cavity with nitrogen gas.



## **CHAPTER FOUR**

### **RESULTS AND DISCUSSION**

## CHAPTER 4

### RESULTS AND DISCUSSION

#### 4.1 DETERMINATION OF THE MAGNETIC PARAMETERS

##### 4.1.1 Isotropic Magnetic Parameters

The vanadyl radical has an electron spin of half which interacts with the vanadyl nucleus which has spin  $I = 7/2$ ; therefore, the EPR spectrum consists of  $(2I + 1)$ , i.e. eight lines.

The spectrum of  $\text{VO}[(\text{CH}_3)_2\text{C}=\text{NNC}(\text{SSCH}_3)_2]$  in toluene at 9.487 GHz was taken at room temperature with DPPH as internal standard and is shown in Fig. 4.1. The isotropic hyperfine constants,  $A_0$  and  $g_0$  were obtained from  $B_M$  for line  $M$  and  $B_{-M}$  for line  $-M$  by equations (1.7) and (1.8).  $A_0$  and  $g_0$  were determined for each pair of  $M$  and  $-M$  lines and averaged over all pairs. The results are given in Table 4.1.

The room temperature spectrum of  $\text{VO}[\text{Sal SB}](\text{Phen})$  in toluene with DPPH as internal standard was taken at 9.496 GHz and is shown in Fig. 4.2. Also the room temperature spectrum of  $\text{VO}[5\text{-MeO Sal SB}](\text{Phen})$  in methylene chloride with DPPH as internal standard was taken at 9.434 GHz and is shown in Fig. 4.3. These spectra were analyzed for the isotropic  $g_0$  and  $A_0$  magnetic parameters as done for  $\text{VO}[(\text{CH}_3)_2\text{C}=\text{NNC}(\text{SSCH}_3)_2]$  and the results are shown in Table 4.1.

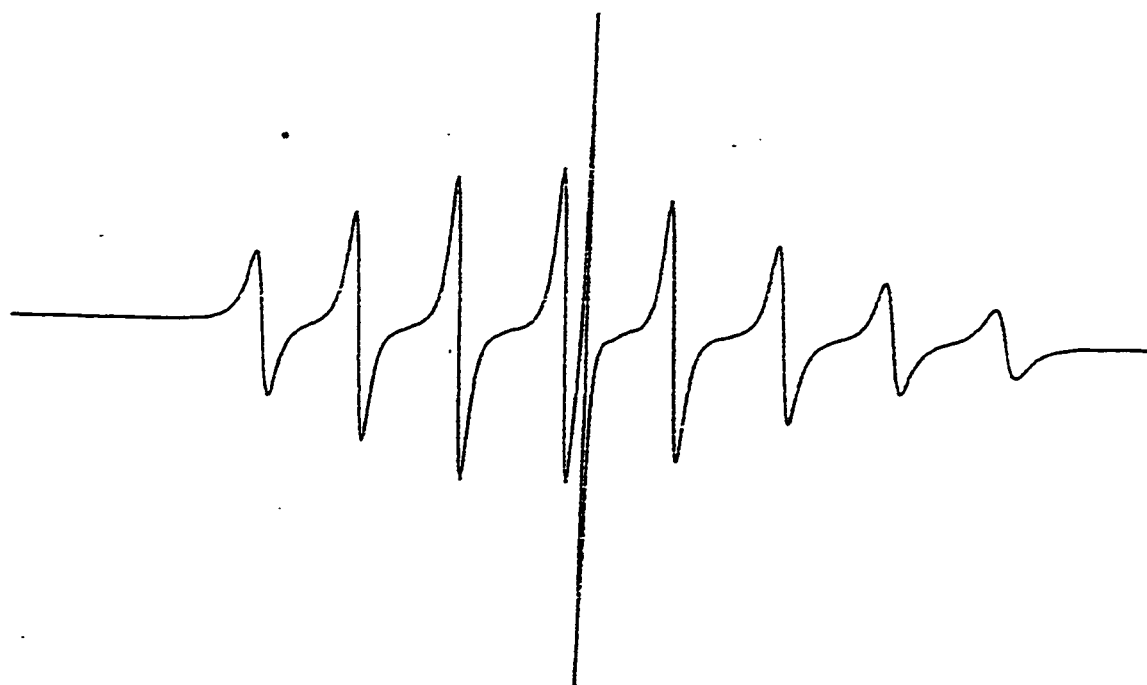
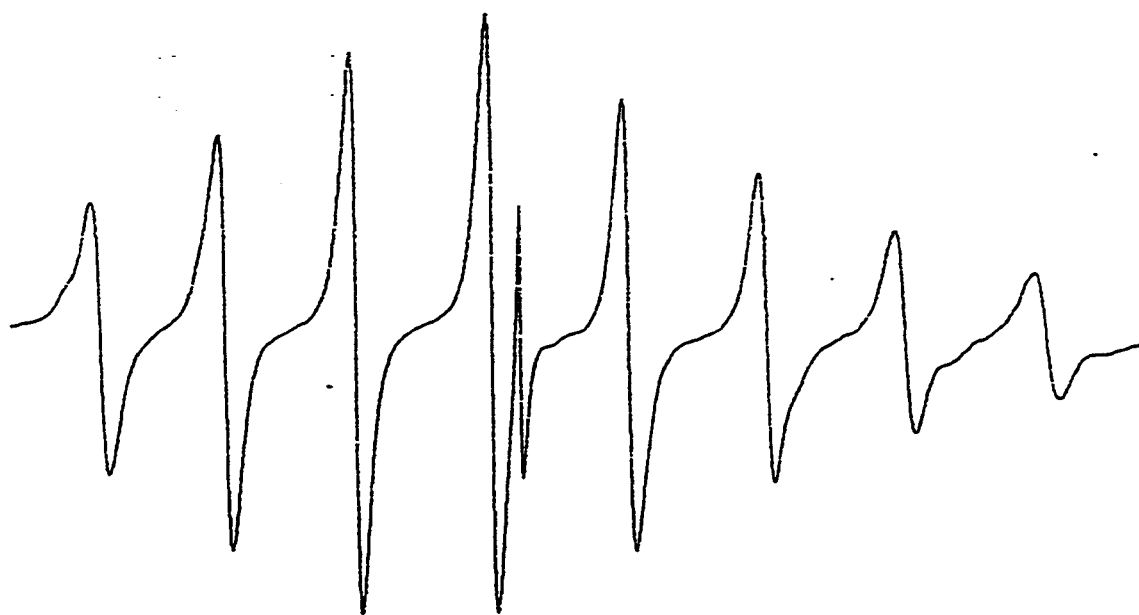
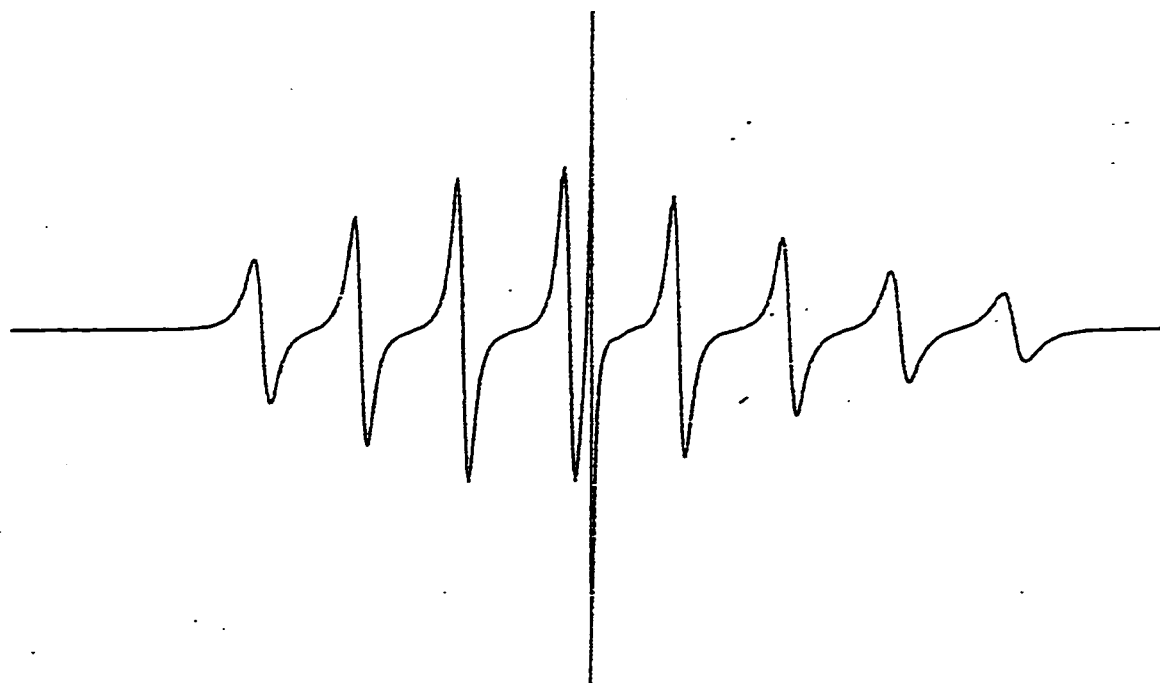


Fig.4.1 : X-band Spectrum of  $\text{VO}[(\text{CH}_3)_2\text{C}=\text{NNCSSCH}_3]_2$  in toluene at room temperature with DPPH as internal standard.



**Fig.4.2 : X-band Spectrum of VO[Sal SB] (Phen) in toluene at room temperature with DPPH as internal standard.**



**Fig.4.3 : X-band Spectrum of VO[5-MeO Sal SB] (Phen) in methylene chloride at room temperature with DPPH as internal standard.**

**Table 4.1: The Isotropic Magnetic Parameters**

Sample	$A_o$ (G)	$g_o$
$VO[(CH_3)_2C=NNCSSH_3]_2^*$	87.14	1.9790
$VO[Sal-SB](Phen)^*$	93.22	1.9787
$VO[5-MeO-Sal SB](Phen)^{**}$	92.44	1.9760

\* in toluene

\*\* in methylene chloride

#### 4.1.2 Anisotropic Magnetic Parameters

The rigid limit spectrum of  $\text{VO}[(\text{CH}_3)_2\text{C}=\text{NNC}(\text{SSCH}_3)_2]$  in toluene was taken at 9.279 GHz and is shown in Fig. 4.4. The anisotropic tensors were determined from this rigid limit spectrum using second-order perturbation theory, and from the isotropic  $A_0$  and  $g_0$  determined from the liquid spectra, as Wilson and Kivelson have done for VOAA{3}.

Spacings II and III, from rigid limit spectrum (Fig. 4.4), are used in equation (1.14) to determine  $A_z$ ,

$$A_z(\text{G}) = \frac{\text{II} + \text{III}}{2} = 160.02 \text{ G.}$$

As the resonant lines for the magnetic field parallel to Z-axis ( $\text{H} \parallel \text{Z}$ ) are concentric around  $g_z$  value. From the two terminal resonant lines in the glass spectrum, Fig. 4.4, which corresponds to  $\text{H} \parallel \text{Z}$  ( $B_{7/2}$  and  $B_{-7/2}$ ) value of  $g_z$  can be obtained as follows:

$$g_z = \frac{h\nu}{\beta_0} \left/ \left[ \frac{B_{7/2} - B_{-7/2}}{2} \right] \right. \quad (4.1)$$

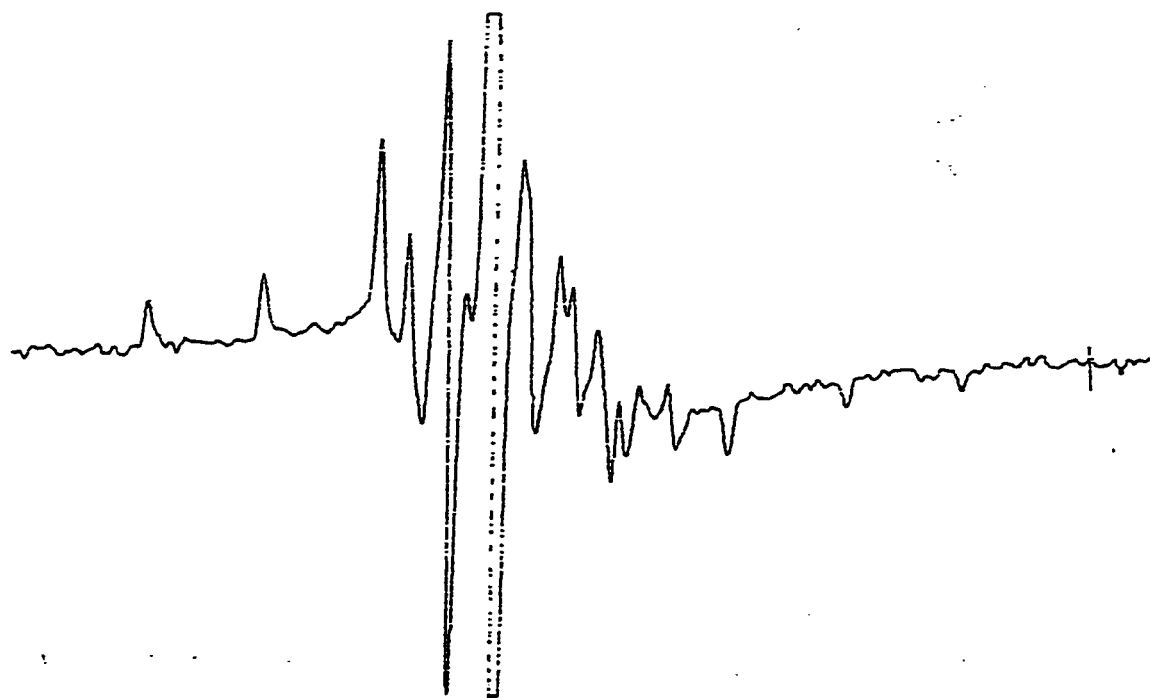


Fig.4.4 : X-band Spectrum of  $\text{VO}[(\text{CH}_3)_2\text{C}=\text{NNC}(\text{S})\text{SCH}_3]_2$  in toluene at  $T = 77 \text{ K}$ .



where

$h$  is Planck's constant

$\nu$  is the microwave frequency in Hz

$\beta_0$  is the Bohr magneton.

The value of  $g_z$  was found to be 1.9603.

Combining the values of  $A_z$  and  $g_z$  obtained from rigid limit spectrum with those of  $A_0$  and  $g_0$  obtained from the liquid spectra in Equations (1.5) and (1.6), values of  $A_x + A_y$  and  $g_x + g_y$  were obtained as follows:

$$A_x + A_y = 3A_0 - A_z = 101.40 \text{ G.} \quad (4.2)$$

$$g_x + g_y = 3g_0 - g_z = 3.9767 \quad (4.3)$$

In fact the rigid limit resonant lines for  $H \parallel Z$  is governed by:

$$\omega_o = \frac{g_z \beta_o B_M}{\hbar} + A_z M + \frac{(A_x^2 + A_y^2)(\frac{63}{4} - M^2)}{4 g_z \beta_o B_M / \hbar} \quad (4.4)$$

which is the case in Eq. (1.13) where  $\theta = 0$ . Substituting  $A_y$  obtained from Eq. (4.2) above in Eq. (4.4) yields  $A_x$ -value which can be used in Eq. (4.2) to calculate the value of  $A_y$ . Moreover, using Eq. (4.4) and resonant lines for  $H \parallel Z$ , the tensors obtained above were further adjusted.

Furthermore, spacing  $I$  is:

$$I \text{ (in Hz)} = \left[ \beta_o B (g_x - g_y) / \hbar \right] + 7/2 (A_x - A_y) \quad (4.5)$$

where  $B$  (in gauss) is calculated from the microwave frequency (in Hz) and  $g_o$  by equation (1.9).

Spacing  $I$  measured from the rigid limit (Fig. 4.4) in gauss, should be used in Eq. (4.5) in Hz.

Substituting  $A_x$  and  $A_y$  values obtained from Eq. (4.5) and values of  $g_y$  from Eq. (4.3) the following expression was obtained:

$$I \text{ (in Hz)} = \left[ \beta_o B(2g_x + g_z - 3g_o)/h \right] + 7/2 (A_x - A_y) \quad (4.6)$$

which is solved to give the  $g_x$  value and then  $g_y$  is also obtained using Eq. (4.3)

Again when  $\theta = \pi/2$  and  $\varphi = 0$  and  $\pi/2$  in Eq. (1.13) yield the following two equations which govern the resonant lines for  $H \parallel X$ -axis and  $H \parallel Y$ -axis respectively.

$$\omega_o = \frac{g_x \beta_o B_M}{h} + A_x M + \frac{(A_x^2 + A_y^2)(A_x^2 + A_z^2)(\frac{63}{4} - M^2)}{8 A_x^2 g_x \beta_o B_M/h} \quad (4.7)$$

$$\omega_o = \frac{g_y \beta_o B_M}{h} + A_y M + \frac{(A_x^2 + A_y^2)(A_y^2 + A_z^2)(\frac{63}{4} - M^2)}{8 A_y^2 g_y \beta_o B_M/h} \quad (4.8)$$

The above two equations were used to verify the calculated values of the  $g$  and  $A$  tensors. The obtained  $g$  and  $A$  values for  $\text{VO}[(\text{CH}_3)_2\text{C}=\text{NNCSSCH}_3]_2$  are listed in Table 4.2.

The spectrum of VO[Sal SB](Phen) in toluene at 77K was taken at 9.287 GHz and is shown in Fig. 4.5. From this spectrum, the three components of the g tensor as well as the three components of the hyperfine tensor were determined using second-order perturbation-theory results as done for  $\text{VO}[(\text{CH}_3)_2\text{C}=\text{NNC}(\text{SSCH}_3)_2]$ . These g and A tensors are shown in Table 4.2.

Also the spectrum of VO[5-MeO Sal SB](Phen) in methylene chloride at 77K was taken at 9.505 GHz and is shown in Fig. 4.6. This spectrum was analyzed for the anisotropic g and A tensors which are shown in Table 4.2.

From the absence of any further splitting of the resonant lines at rigid limit and the constant values (within experimental error) of the isotropic g and A magnetic parameters for different M and -M pairs, as shown in Table 4.3, it is concluded that there is no V-V bond in  $\text{VO}[(\text{CH}_3)_2\text{C}=\text{NNC}(\text{SSCH}_3)_2]$  solution, thus ruling out the dimerization through V-V interactions as suggested by others [1].

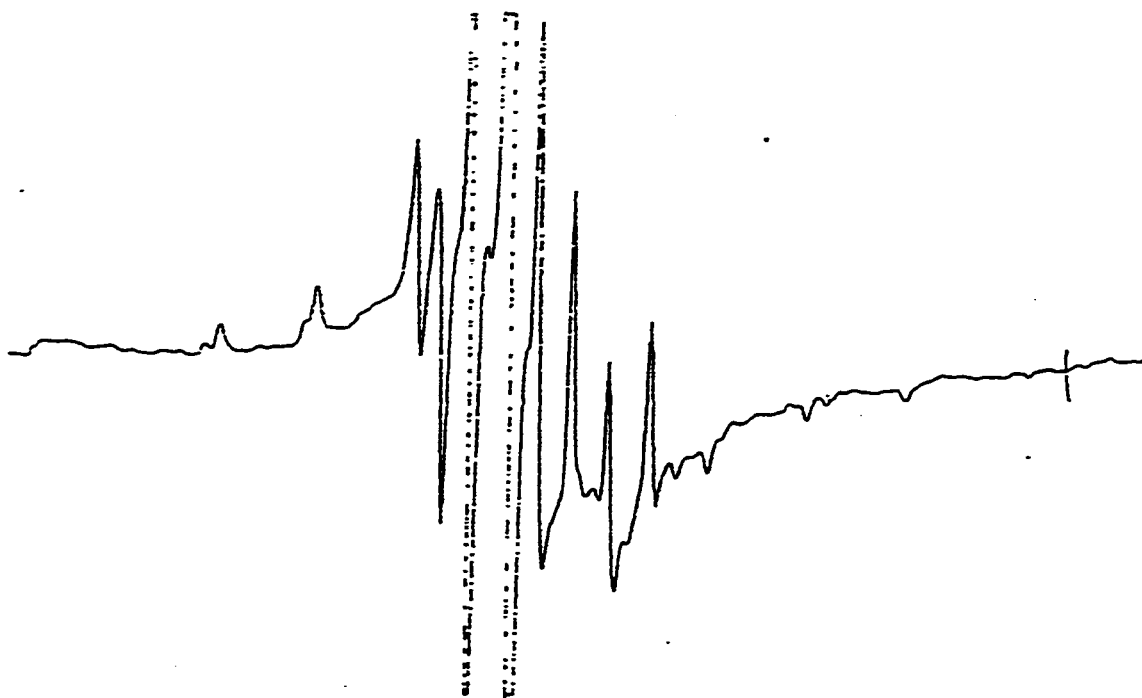


Fig.4.5 : X-band Spectrum of VO[Sal SB] (Phen) in toluene at  
T = 77 K.

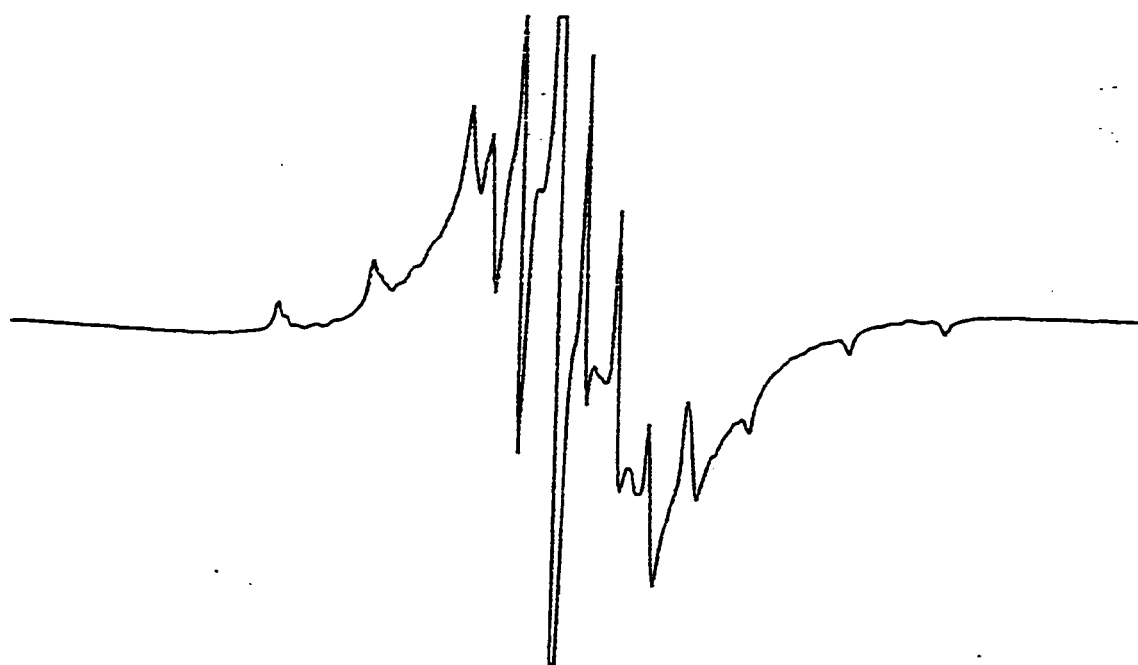


Fig.4.6 : X-band Spectrum of VO[5-MeO Sal SB] (Phen) in methylene chloride at T = 77 K.

Table 4.2: The Anisotropic Magnetic Parameters

Sample	$g_z$	$g_y$	$g_x$	$A_x$ (G)	$A_y$ (G)	$A_z$ (G)
$VO(CH_3)_2C=NNSSCH_3)_2$ *	1.9603	1.9846	1.9915	46.91	54.33	160.02
$VO[Sal-SB](Phen)$ *	1.9534	1.9887	1.9970	51.76	62.94	165.21
$VO[5-MeO-Sal-SB](Phen)$ **	1.9572	1.9730	1.9980	46.75	64.05	166.53

\* in toluene.

\*\* in methylene chloride

**Table 4.3: Isotropic  $g$  and  $A$  for  $\text{VO}[(\text{CH}_3)_2\text{C}=\text{NCSCH}_3]_2$   
in toluene**

<b>M</b>	<b><math>A_o</math> (G)</b>	<b><math>g_o</math></b>
<b>7/2</b>	<b>86.98</b>	<b>1.9790</b>
<b>5/2</b>	<b>87.09</b>	<b>1.9790</b>
<b>3/2</b>	<b>87.02</b>	<b>1.9790</b>
<b>1/2</b>	<b>87.45</b>	<b>1.9791</b>



## 4.2 MOTIONAL NARROWING ANALYSIS

### 4.2.1 $\text{VO}[(\text{CH}_3)_2\text{C}=\text{NNC}(\text{SCH}_3)_2]$ :

The spectra in Fig. 4.7 are those of  $\text{VO}[(\text{CH}_3)_2\text{C}=\text{NNC}(\text{SCH}_3)_2]$  in toluene at 9 GHz. The ESR spectra were taken over a temperature range (312.8 - 239.4 K) . This free radical has an electron spin (1/2) which interacts with the vanadyl nucleus which has spin  $I = 7/2$ ; therefore, the ESR spectrum consists of eight lines each corresponding to a nuclear spin magnetic quantum number  $M$ :

$$M = I, I - 1, \dots, -I$$

The line width parameter,  $T_2$  (in gauss<sup>1</sup>), of each of these Lorentzian hyperfine lines can be described by an expansion in  $M$ , the component of the nuclear spin along the direction of the applied magnetic field given by equation (1.23).

The lines widths and the peak to peak heights are obtained experimentally utilizing the computer graphic display which facilitates on screen line width measurements. After measuring the line widths of each of these lines, the widths are then entered into the computer program written for Eq. (1.23) where experimental values of  $A$ ,  $B$  and  $C$  are obtained by least square fitting. These  $B$  and  $C$  values for

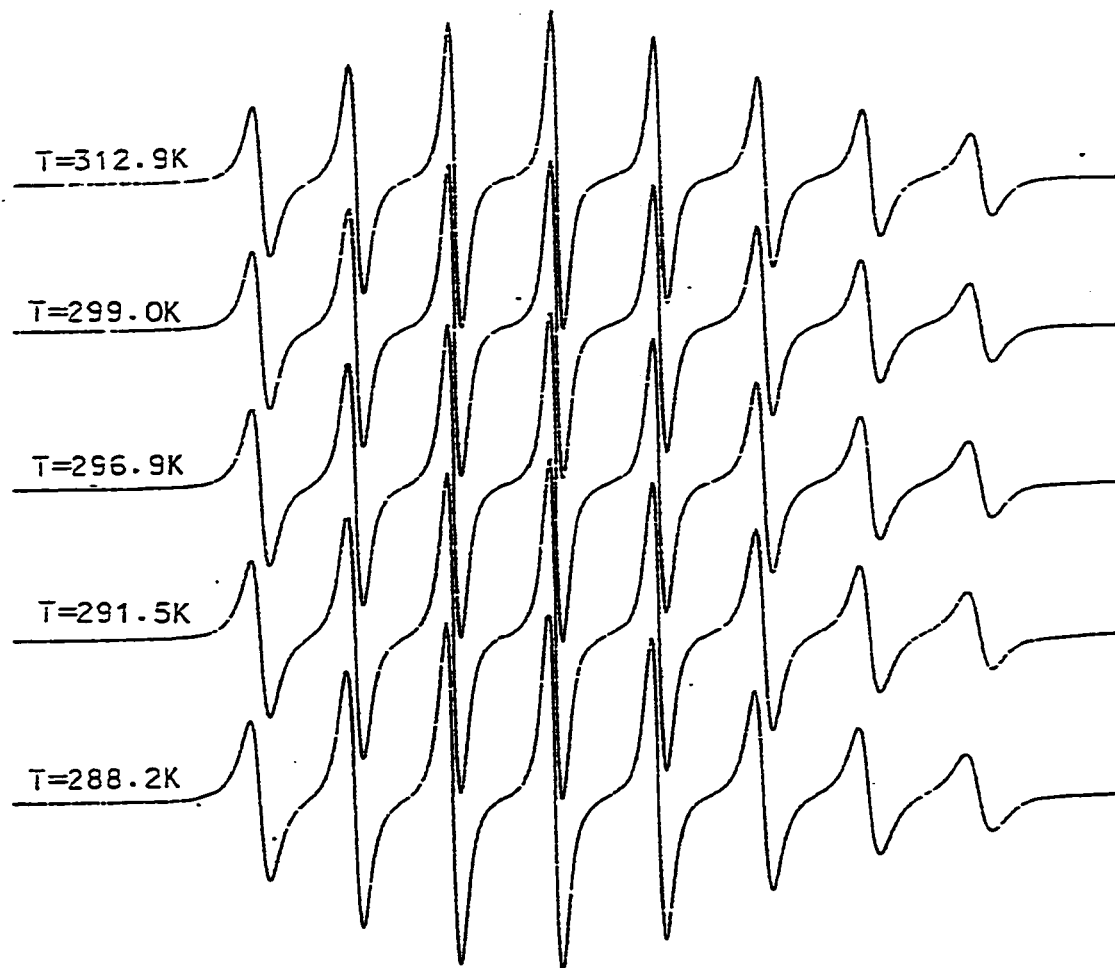


Fig.4.7 : Experimental Spectra of  $\text{VO}[(\text{CH}_3)_2\text{C}=\text{NNCSSCH}_3]_2$  in toluene.

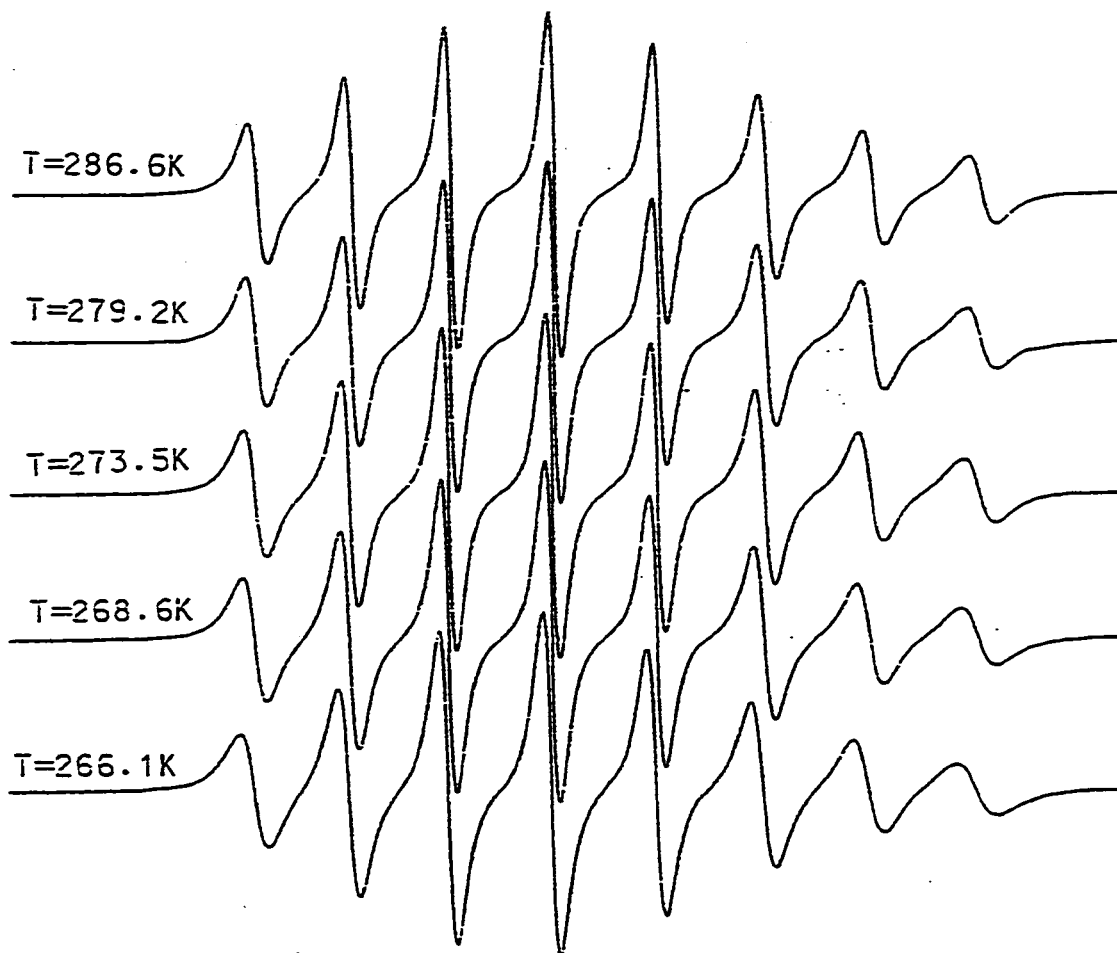
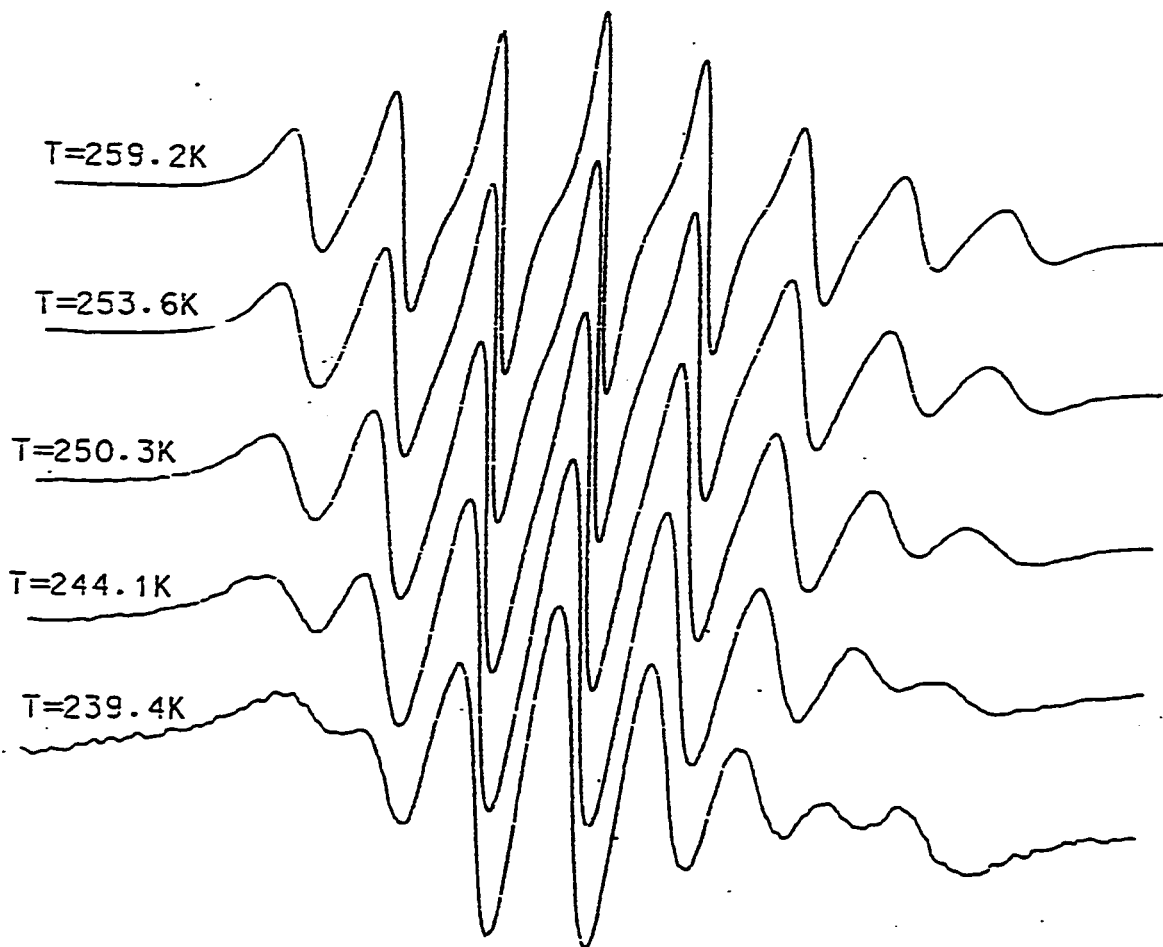


Fig.4.7 : Experimental Spectra of  $\text{VO}[(\text{CH}_3)_2\text{C}=\text{NNCSSH}_3]_2$  in toluene.



**Fig.4.7 : Experimental Spectra of  $\text{VO}[(\text{CH}_3)_2\text{C}=\text{NNCSSCH}_3]_2$  in toluene.**

different temperatures are shown in Table 4.4 and Fig. 4.8 shows the C versus B for  $\text{VO}[(\text{CH}_3)_2\text{C}=\text{NNC}(\text{SSCH}_3)_2]$  at different temperatures.

In order to determine the anisotropy of rotation (N) and the axis of rotation, the theoretical calculations of B and C coefficients which are given by the following equations [34] were used. These equations were adopted from the motional-narrowing analysis of Freed et al. [4,5,6].

$$C_0 = \frac{8}{3} - \left[ 1 + (\omega_0 \tau_0)^2 \right]^{-1} - \frac{1}{\{3 [1 + (\omega_0 \tau_0)^2]\}} \quad (4.9)$$

$$C_2 = \frac{8}{3} - \left[ 1 + (\omega_2 \tau_2)^2 \right]^{-1} - \frac{1}{\{3 [1 + (\omega_2 \tau_2)^2]\}} \quad (4.10)$$

$$C = \left[ \frac{2}{\sqrt{30}} \right] (0.8\pi)^2 (D_0^2 \tau_0 C_0 + 2D_2^2 \tau_2 C_2) \quad (4.11)$$

$$B_0 = \frac{16}{3} + \frac{4}{\left[ 1 + (\omega_0 \tau_0)^2 \right]} \quad (4.12)$$

$$B_2 = \frac{16}{3} + \frac{4}{\left[ 1 + (\omega_2 \tau_2)^2 \right]} \quad (4.13)$$

**Table 4.4: B and C for VO[(CH<sub>3</sub>)<sub>2</sub>C=NNCSSH<sub>3</sub>]<sub>2</sub>**

**in toluene**

<b>t (°C)</b>	<b>B (G)</b>	<b>C (G)</b>
18.3	0.596	0.359
15.0	0.599	0.360
13.4	0.654	0.405
6.0	0.747	0.492
0.3	0.832	0.564
-7.1	0.960	0.669
-14.0	1.110	0.785
-19.6	1.250	0.913
-22.9	1.355	1.003

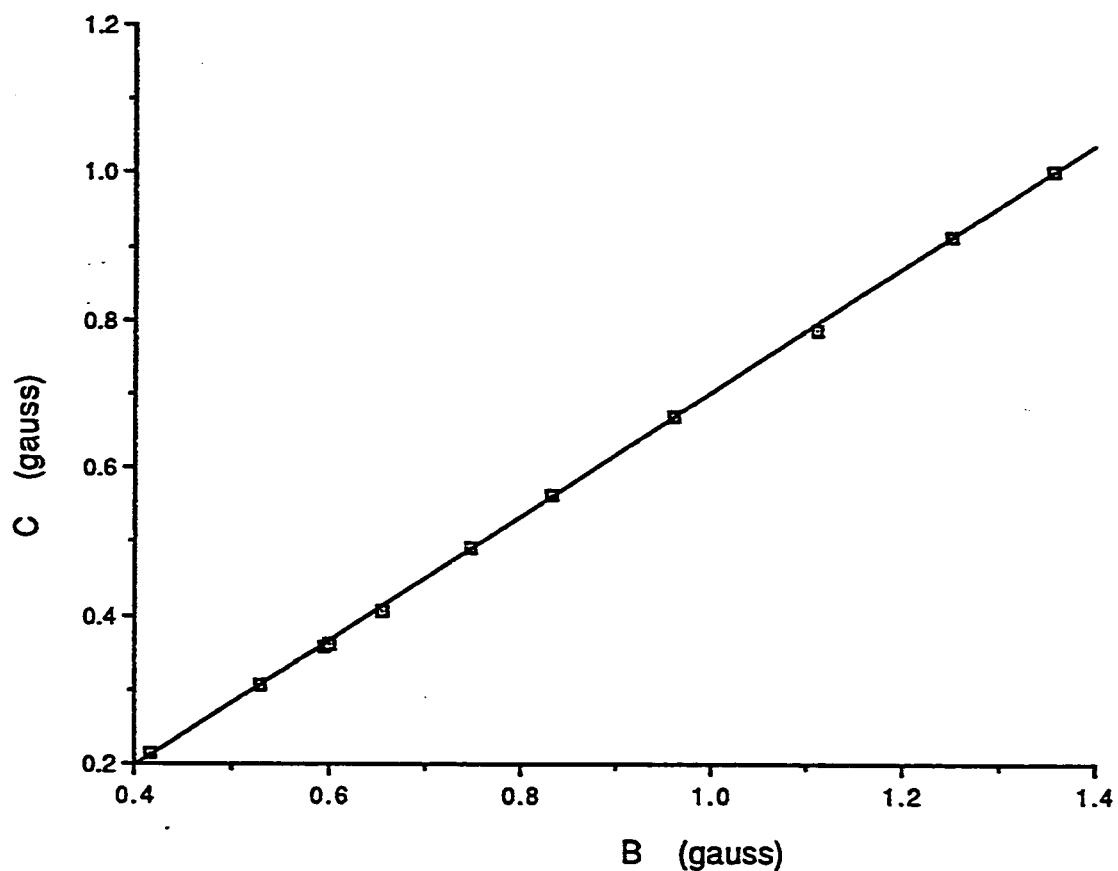


Fig. 4.8 : C vs. B (experimental) plot of  $\text{VO}[(\text{CH}_3)_2\text{C}=\text{NNCSSCH}_3]_2$  in toluene at different temperatures.

$$B = \left( \frac{-2}{\sqrt{3}v} \right) (0.1 \pi m_0) (g_1 D_0 \tau_0 B_0 + 2g_2 D_2 \tau_2 B_2) \quad (4.14)$$

The magnetic parameters  $g$ 's and  $A$ 's for  $\text{VO}[(\text{CH}_3)_2\text{C}=\text{NNCSSCH}_3]_2$  necessary for the simulation of  $A$ ,  $B$  and  $C$ , are taken from the first part of this chapter and given below:

$$g_e = 2.00232$$

$$g_x = 1.9915$$

$$g_y = 1.9846$$

$$g_z = 1.9603$$

$$g_0 = \frac{g_x + g_y + g_z}{3}$$

$$g_1 = (g_z - g_0) \left( \frac{3}{2} \right)^{\frac{1}{2}}$$

$$g_2 = \frac{(g_x - g_y)}{2}$$

$$A_x = 46.91 \text{ G.}$$

$$A_y = 54.33 \text{ G.}$$



$$A_z = 160.02 \text{ G.}$$

$$A_o = \frac{(A_x + A_y + A_z)}{3}$$

$$\nu = 1.764097 \times 10^7 \text{ Sec}^{-1} \text{ G}^{-1}$$

$$\omega_o = 2\pi\nu$$

$$\nu_p = \nu \frac{g_o}{g_e}$$

$$\omega_x = \frac{A_o \nu_p}{2}$$

$$D_o = (A_z - A_y) \left[ \frac{|\nu_p|}{2\pi} \right] \left( \frac{3}{8} \right)^{\frac{1}{2}}$$

$$D_2 = (A_x - A_y) \left[ \frac{|\nu_p|}{8\pi} \right] \text{ MHz}$$

$$\tau_o = \tau_R N^{\frac{1}{2}}$$

$$\tau_2 = \frac{3\tau_o}{(1+2N)}$$

The theoretical calculations of B and C coefficients are performed by

varying  $\tau_R$  in equations (4.9 to 4.14). The program written for equations (4.9-4.14) is known as the ABC program. While performing theoretical simulation at the beginning we mainly look at the C/B ratio with the anisotropic rotational diffusion and reorientation. Basically, the simulation of these curves using equations (4.9-4.14) involves the fitting of three parameters the C/B ratio, the principal axis of rotation ( $\bar{Z}$ -axis) and N.

Usually the approximate ratio of C/B gives some hint on the  $\bar{Z}$ -axis. Value of N is then varied to move the upper portion of the curve to approach the experimental points.

Fig. 4.9 shows simulation with  $\bar{Z} = Y$  for different N values. Curves in Fig. 4.9 are generated with N values vary from 0.5 to 7.0. Higher N values have upward shift and the lower N values have downward shift. The uniqueness of N is partly dependent on the uncertainty of experimental points. On the basis of the precision of our experiment, N values 7.0, 5.0, 3.5, 2.5, 1.0, and 0.5 are clearly separated from each other. N thus determined has a precision  $\pm 0.5$ . The curve with N = 2.5 gives the best simulation.

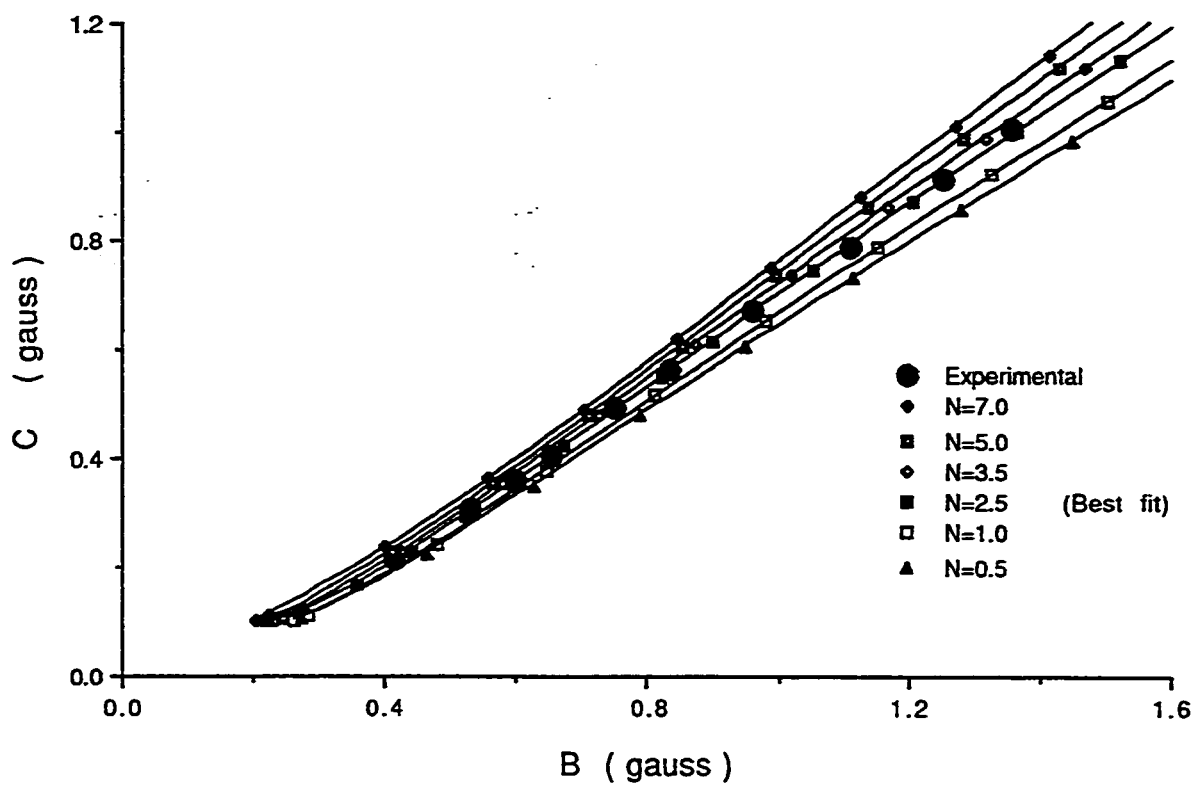


Fig.4.9 : Effect of varying N for  $\text{VO}[(\text{CH}_3)_2\text{C}=\text{NNCSSCH}_3]_2$  in toluene. Curves are simulated with  $\bar{Z} = Y$ .

Next we look at axes  $\bar{Z} = X$  and  $\bar{Z} = Z$ . Fig. 4.10 shows simulation with  $\bar{Z} = X$ . Higher N values shift the curves downward. All the curves are below the experimental curve and changes in N are not able to bring the curves to approach the experimental points.

Fig. 4.11 shows simulation with  $\bar{Z} = Z$ . This simulation is very insensitive to changes in N. The curves for N equal to 7.0, 5.0, 3.0 and 0.7 are superimposed.

The effect of varying N is shown in Figs. 4.9, 4.10 and 4.11. For  $\bar{Z} = Y$ , larger N shifts the whole curve upward as shown in Fig. 4.9. Fig. 4.10 shows the effect of N for axis  $\bar{Z} = X$  where larger N shifts the curve downward. Fig. 4.11 shows the effect of N with  $\bar{Z} = Z$  where it is observed that the simulation is very much insensitive to N.

Thus it is determined from simulation that  $\text{VO}[(\text{CH}_3)_2\text{C}=\text{NNCSSCH}_3]_2$  in toluene experiences anisotropic rotational diffusion at an axis  $\bar{Z} = Y$  with  $N = 2.5 \pm 0.5$ .

In the absence of external influence, an ellipsoid would always prefer to rotate along its longest axis, since the energy barrier for rotation along the longest axis is less than those for the other two axes. This is actually what is observed.  $\text{VO}[(\text{CH}_3)_2\text{C}=\text{NNCSSCH}_3]_2$  has a preferential rotation axis ( $\bar{Z} = Y$ ) over the other two axes.

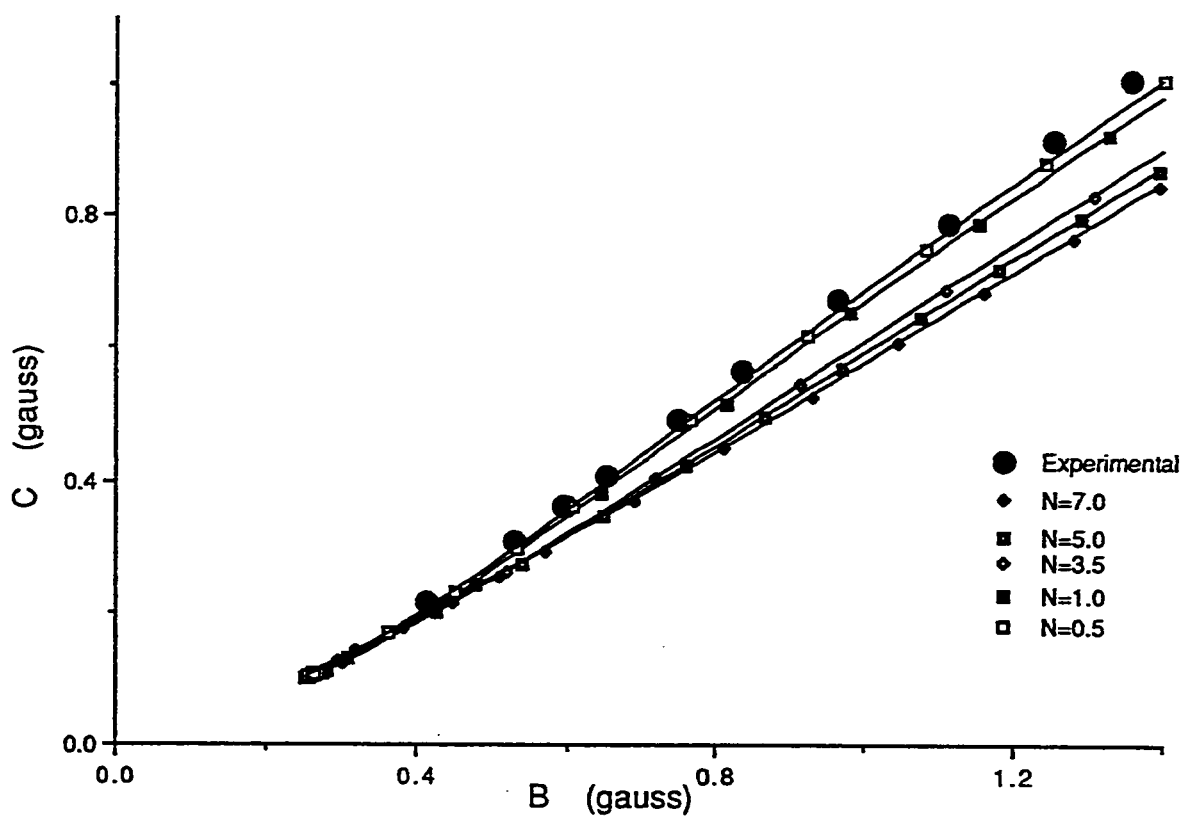


Fig.4.10 : Effect of varying N for  $\text{VO}[(\text{CH}_3)_2\text{C}=\text{NNC}(\text{SCH}_3)_2]$  in toluene. Curves are simulated with  $\bar{Z} = X$ .

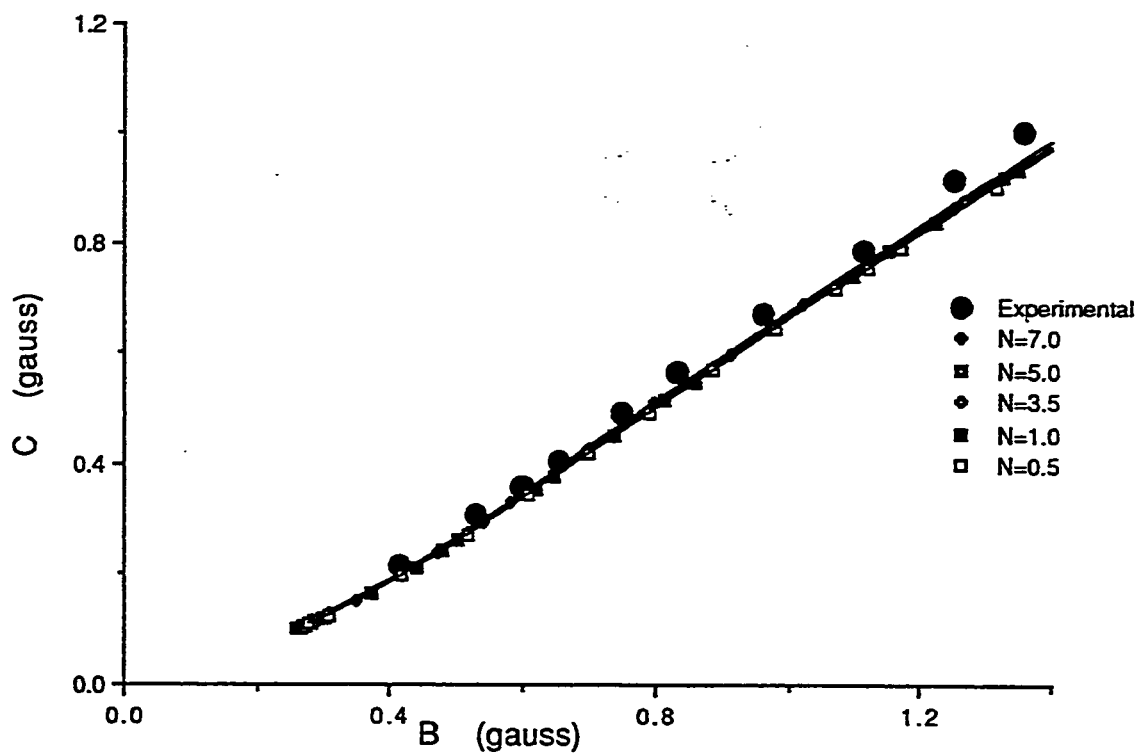


Fig.4.11 : Effect of varying N for  $\text{VO}[(\text{CH}_3)_2\text{C}=\text{NNC}(\text{SCH}_3)_2]$  in toluene. Curves are simulated with  $\bar{Z} = Z$ .

#### 4.2.2 VO[5-MeO Sal SB](Phen)

The spectra in Fig. 4.12 are those of VO[5-MeO Sal SB](Phen) in methylene chloride taken over a temperature range of 303.2 - 197.2 K. This free radical shows eight lines spectrum as expected. The line width for each of these Lorentzian hyperfine lines were measured using the computer graphic display which facilitates on screen line width measurements. The line width of each line are entered into the data file of the computer program written for Eq.(1.23) which calculates the values of B and C . These B and C values are shown in Table 4.5 and Fig.4.13 shows C versus B plot of VO[5-MeO Sal SB](Phen) at different temperatures.

The theoretical values of B and C are simulated using the ABC program. The magnetic parameters needed for this simulation are taken from first part of this chapter (Table 4.2).

Fig. 4.14 shows simulation with  $\bar{Z} = Y$  and N is shown to vary from 0.5 to 7.0. Higher N values have an upward shift and lower N values have downward shift. On the basis of the precision of our experiment, N values 7.0, 5.0, 3.0, 1.7, 1.0 and 0.5 are clearly separated from each other. N thus determined has a precision of  $\pm 0.5$ . The curve (N = 1.7) is the best fit.

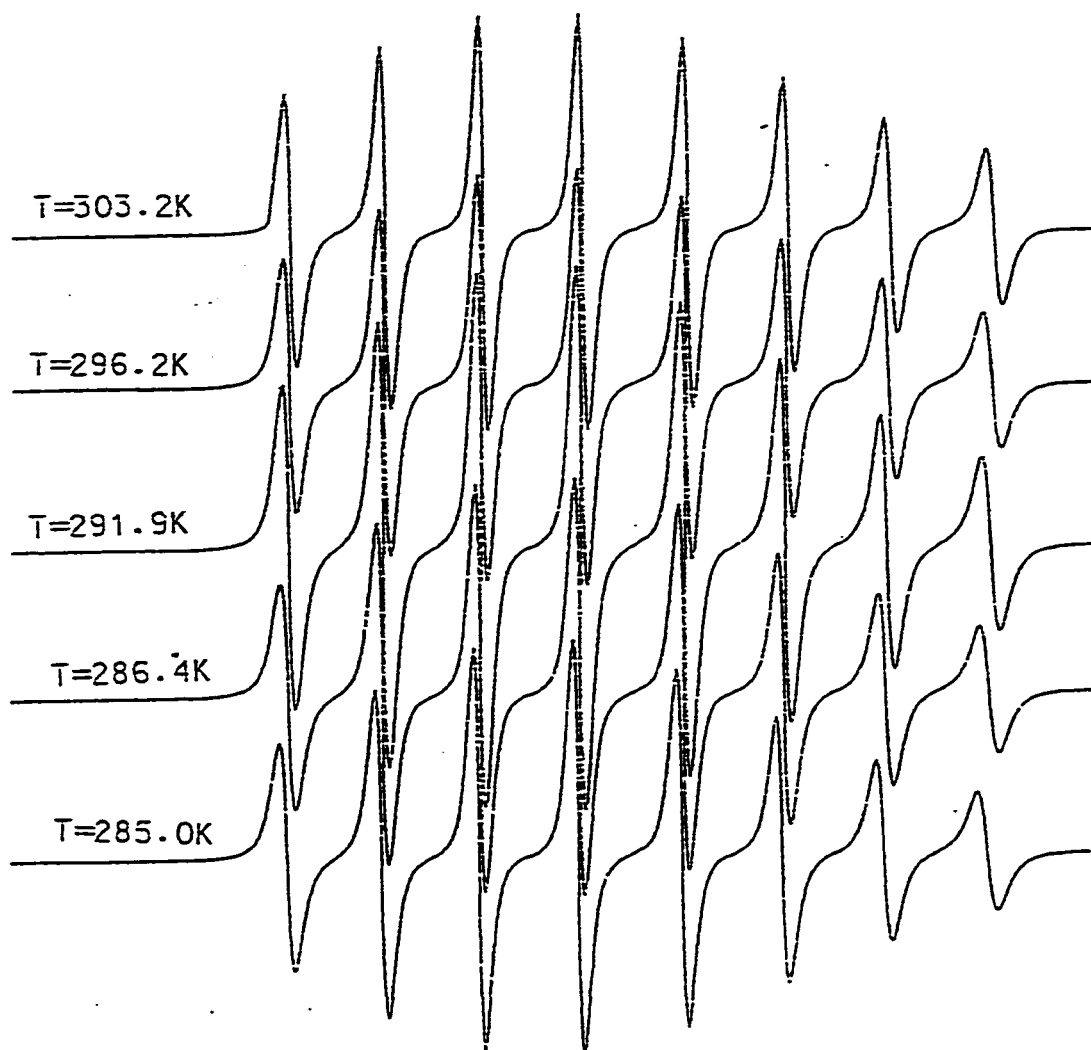


Fig.4.12 : Experimental spectra of VO[5-MeO Sal SB](Phen) in methylene chloride.



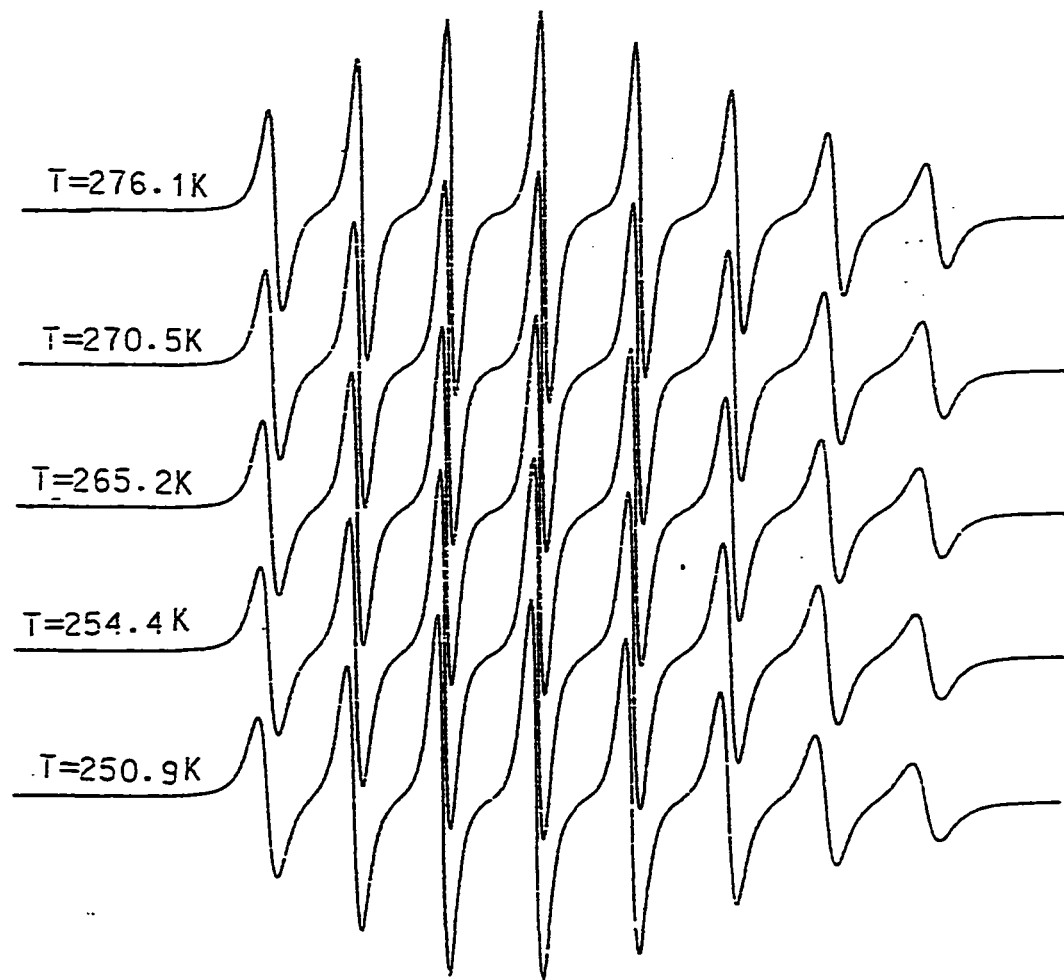


Fig.4.12 : Experimental spectra of VO[5-MeO Sal SB](Phen) in methylene chloride.

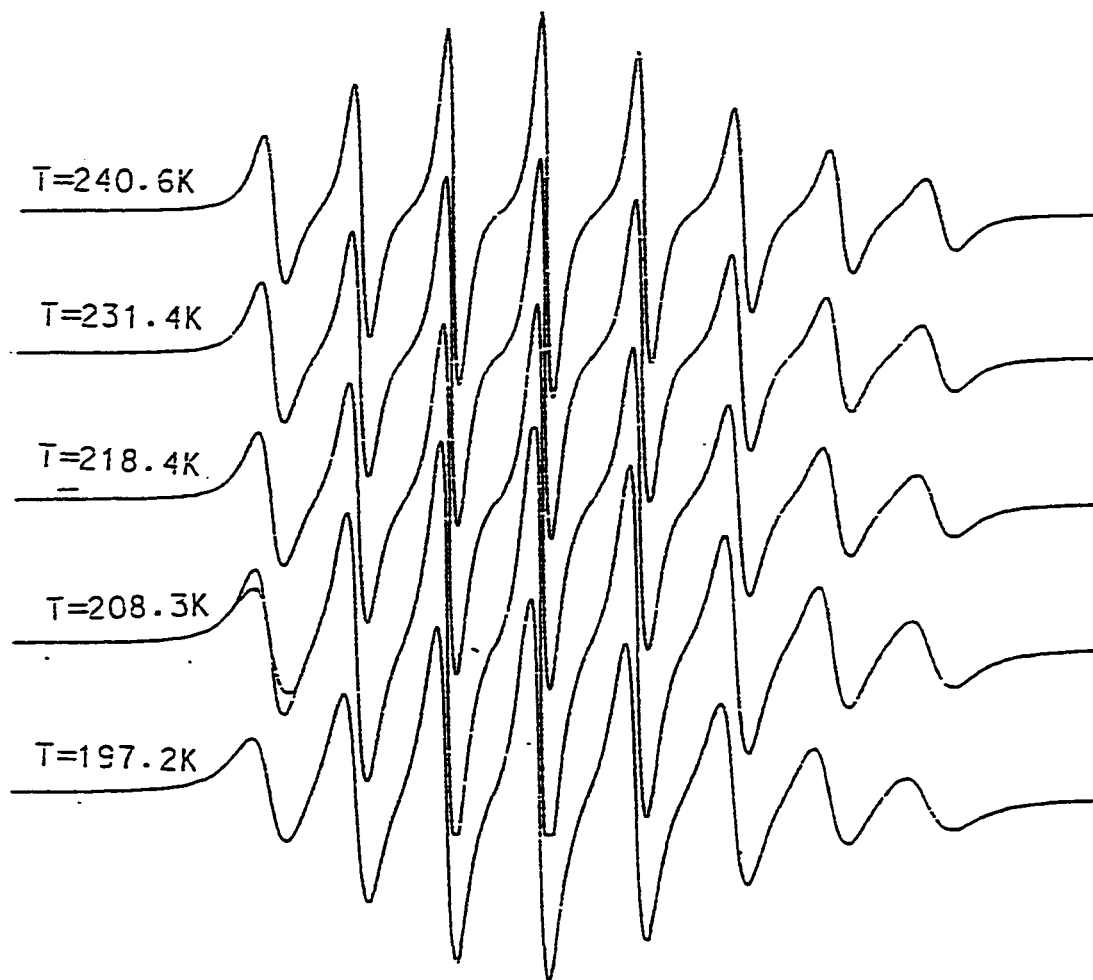


Fig.4.12 : Experimental spectra of VO[5-MeO Sal SB](Phen) in methylene chloride.

**Table 4.5: B and C for VO[5-MeO Sal SB](Phen)  
in methylene chloride**

T (°C)	B (G)	C (G)
11.8	0.947	0.625
5.1	1.029	0.680
2.9	1.062	0.703
-2.7	1.133	0.779
-5.5	1.186	0.805
-18.8	1.443	1.010
-22.8	1.529	1.090
-24.5	1.5175	1.122
-30.0	1.733	1.244
-32.6	1.819	1.307
-41.8	2.171	1.475

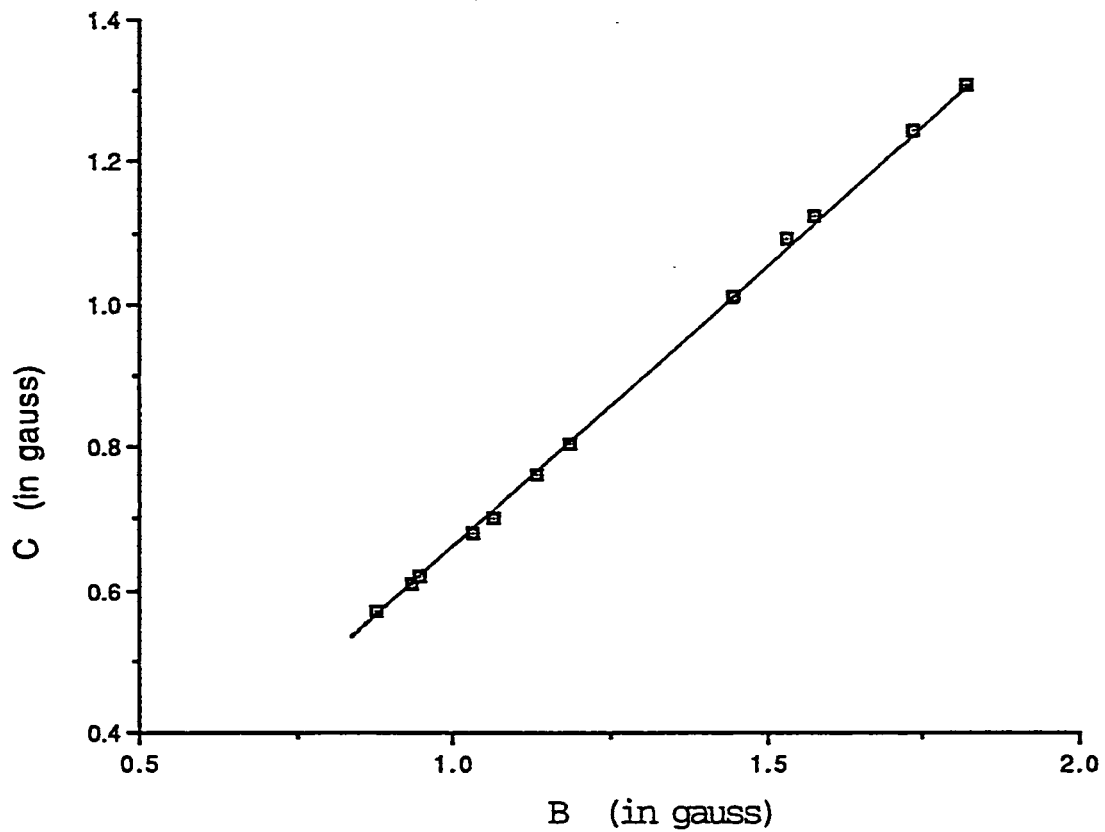


Fig.4.13 : C vs. B (experimental) plot of VO[5-MeO Sal SB](Phen) in methylene chloride at different temperatures.

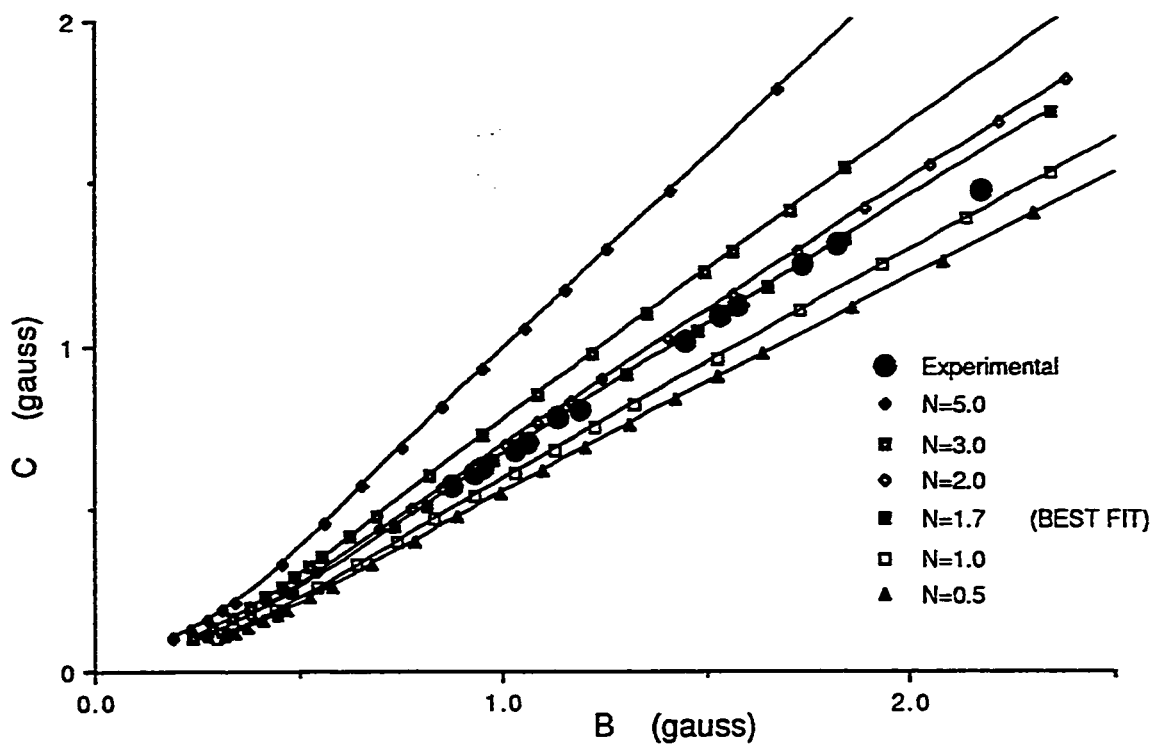


Fig.4.14 : Effect of varying N for VO[5-MeO Sal SB] (Phen) in methylene chloride. Curves are simulated with  $\bar{Z} = Y$ .

In order to see the effect of varying N on different axes, plots for  $\bar{Z} = X$  and  $\bar{Z} = Z$  were performed. Fig. 4.15 shows simulation with  $\bar{Z} = Z$ . Higher N values shift the curves upward, all the curves are below the experimental curve and changes in N values are not able to bring the curves up to approach the experimental points.

Fig. 4.16 shows simulation with  $\bar{Z} = X$ . Higher N values shift the curves downward. The curve simulated with  $N = 0.5$  gives the best fit to the experimental curve within the experimental error. This value of  $N = 0.5$  for  $\bar{Z} = X$  compared to  $N = 1.7$  for  $\bar{Z} = Y$  indicates that the molecule is rotating slower at the X-axis than the Y-axis.

The effect of varying N is shown in Figs. 4.14, 4.15 and 4.16. For  $\bar{Z} = Y$ , higher N value shifts the whole curve upward as shown in Fig. 4.14. Fig. 4.15 shows the effect of N for axis  $\bar{Z} = Z$  where larger N shifts the curve downward. Fig. 4.16 shows the effect of N with  $\bar{Z} = X$  where larger N shifts the curve downward with best fit of  $N = 0.5$  which indicates slower rotation at the X-axis than the Y-axis.

Thus it is determined from simulation that VO[5-MeO Sal SB](Phen) in methylene chloride experiences anisotropic rotational diffusion at an axis  $\bar{Z} = Y$  with  $N = 1.7$ .

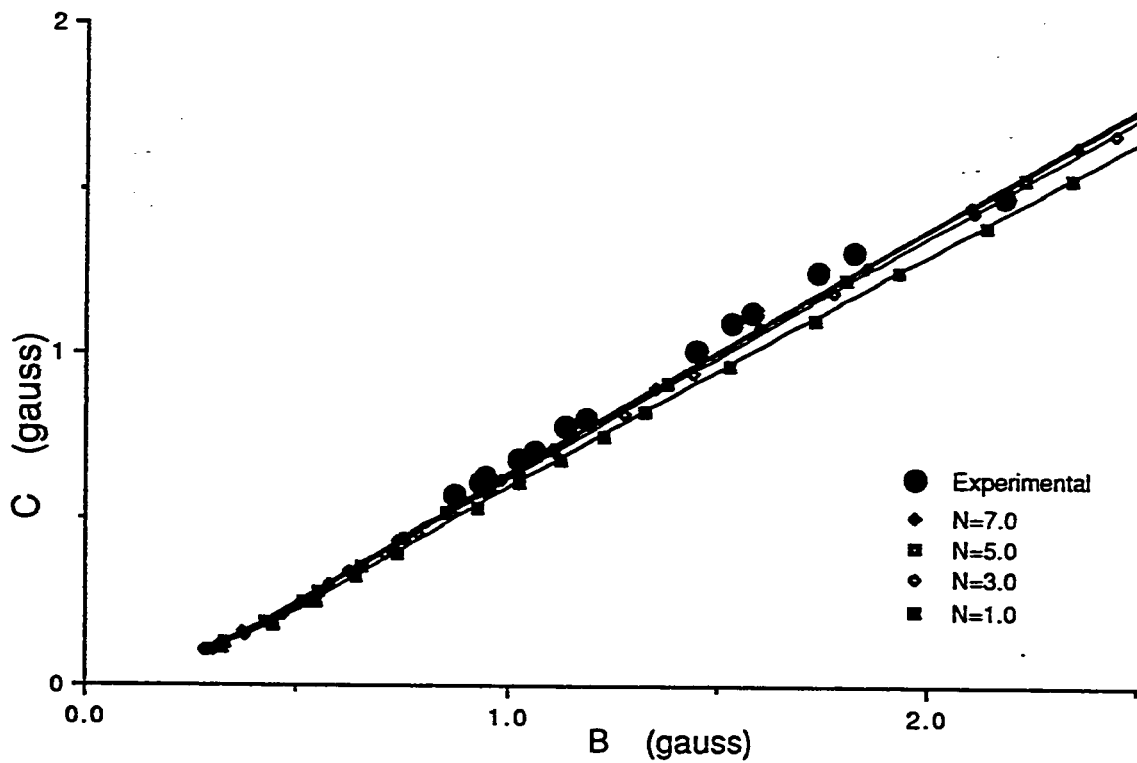


Fig.4.15 : Effect of varying N for VO[5-MeO Sal SB] (Phen) in methylene chloride. Curves are simulated with  $\bar{Z} = Z$ .

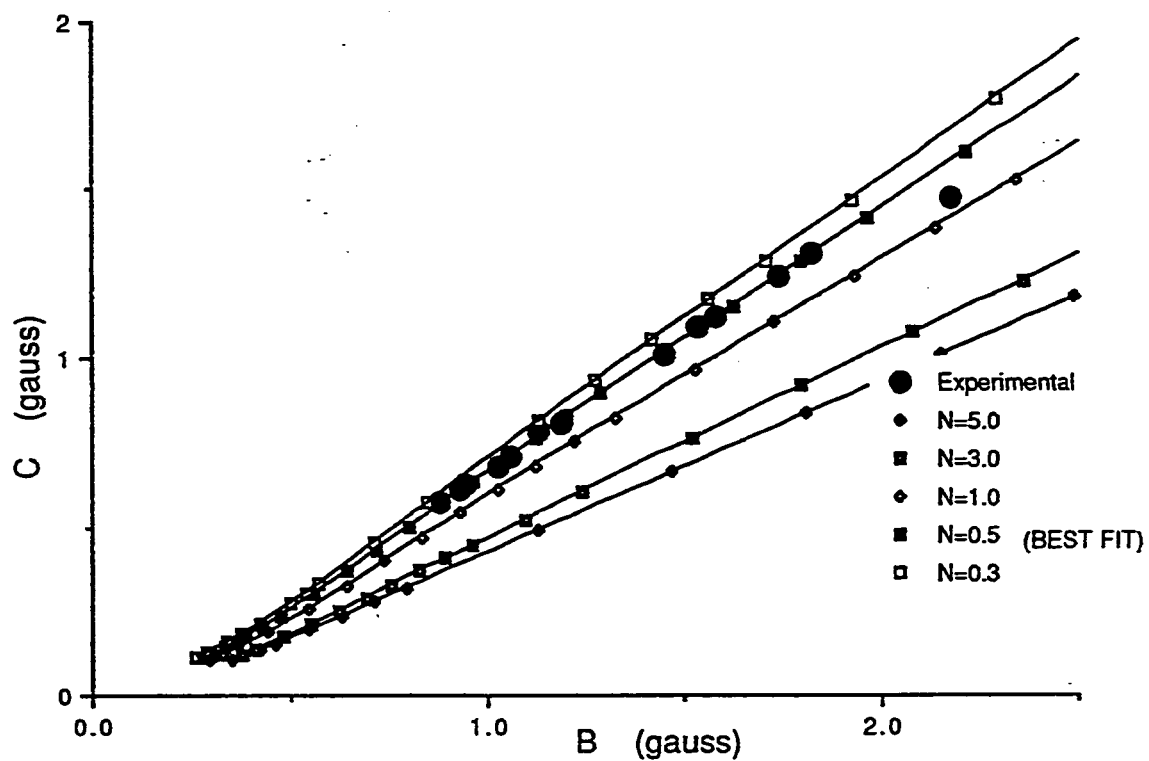


Fig.4.16 : Effect of varying N for VO[5-MeO Sal SB] (Phen) in methylene chloride. Curves are simulated with  $\bar{Z} = X$ .



Also this molecule has a preferential rotation axis ( $\bar{Z} = Y$ ) over the other two axes, as the energy barrier is comparatively less than that for the other two axes. In other words this molecule in methylene chloride is rotating along the Y-axis 1.7 times faster than along the other two axes.

### 4.3 ANISOTROPIC INTERACTION PARAMETER ( $\kappa$ ):

#### 4.3.1 VO[(CH<sub>3</sub>)<sub>2</sub>C=NNCSSH<sub>3</sub>]<sub>2</sub>:

Using the value of N in the ABC program,  $\tau_R$  values can be simulated from the line widths of the experimental spectra at different temperatures. Simulation of  $\tau_R$  values for VO[(CH<sub>3</sub>)<sub>2</sub>C=NNCSSH<sub>3</sub>]<sub>2</sub> in toluene at different temperatures is carried out with N = 2.5 along  $\bar{Z} = Y$  axis. The values of  $\tau_R$  so obtained are presented in Table 4.6. Fig. 4.17 shows  $\tau_R$  as a function of  $\eta/T$  for the spectra taken at higher temperatures, i.e. above the freezing point of toluene. The values of the viscosity of toluene at different temperatures are obtained from the International Critical Tables [36]. It is found that  $\tau_R$  is linear in  $\eta/T$ . The slope of  $\tau_R$  vs  $\eta/T$  for VO[(CH<sub>3</sub>)<sub>2</sub>C=NNCSSH<sub>3</sub>]<sub>2</sub> at 9.38 GHz is  $2.01 \times 10^{-6}$  sec KP<sup>-1</sup>. For our systems this correlation time can be expressed in terms of Stokes-Einstein relation.

$$\tau_R = \frac{4}{3} \left[ \frac{\pi r_o^3}{k_B} \right] \left( \frac{\eta}{T} \right)^\kappa \quad (4.15)$$

Table 4.6:  $\tau_R$  and  $\eta/T$  Values for  $\text{VO}[(\text{CH}_3)_2\text{C}=\text{NNCSSCH}_3]_2$   
in toluene at different temperatures

T (K)	$\eta/T$ ( $\text{PK}^{-1}$ )	$\tau_R$ (sec)
291.5	$2.058 \times 10^{-6}$	$3.017 \times 10^{-11}$
288.2	$2.171 \times 10^{-6}$	$3.242 \times 10^{-11}$
286.6	$2.229 \times 10^{-6}$	$3.355 \times 10^{-11}$
279.2	$2.528 \times 10^{-6}$	$3.950 \times 10^{-11}$
273.2	$2.798 \times 10^{-6}$	$4.500 \times 10^{-11}$
266.1	$3.216 \times 10^{-6}$	$5.340 \times 10^{-11}$
259.2	$3.690 \times 10^{-6}$	$6.300 \times 10^{-11}$
253.6	$4.152 \times 10^{-6}$	$7.225 \times 10^{-11}$
250.3	$4.465 \times 10^{-6}$	$7.850 \times 10^{-11}$

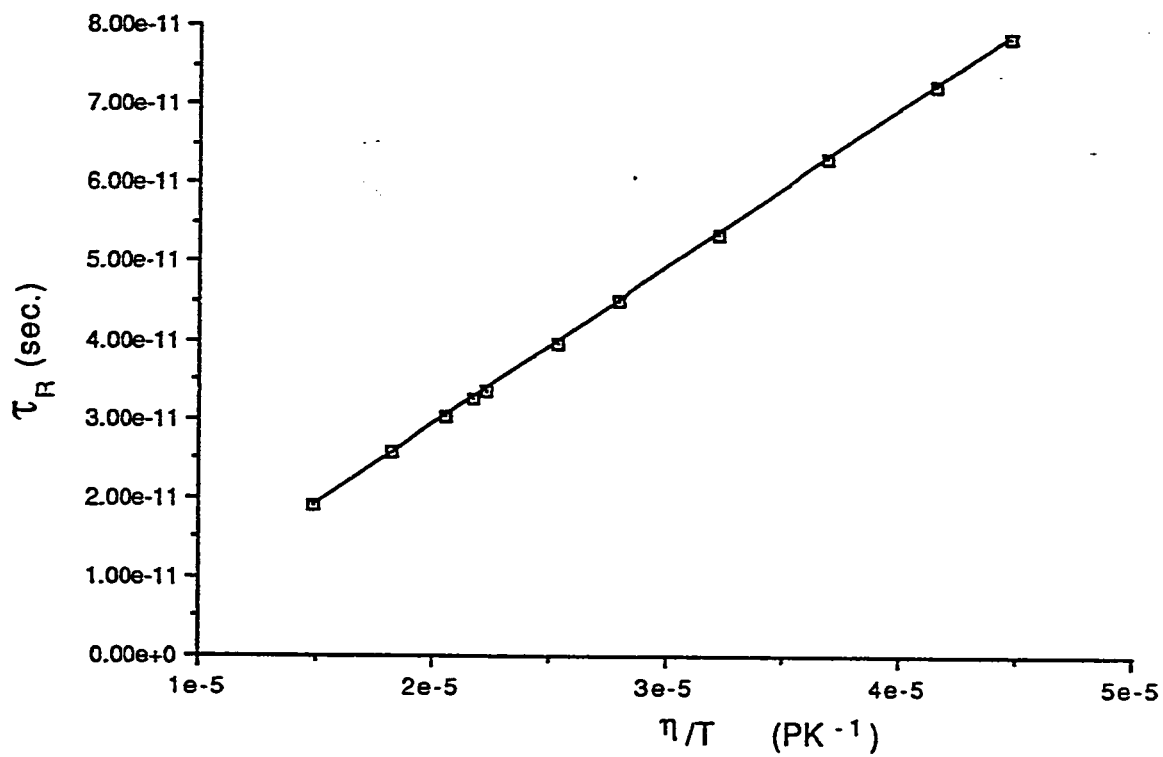


Fig.4.17 :  $\tau_R$  vs  $\eta/T$  plot for  $\text{VO}[(\text{CH}_3)_2\text{C}=\text{NNCSSCH}_3]_2$  in toluene.

where  $k_B$  is the Boltzmann constant,  $T$  the absolute temperature in K,  $\eta$  the coefficient of shear viscosity of solvent in poise,  $\frac{4}{3} \pi r_o^3$  the hydrodynamic molecular volume in  $\text{\AA}^3$ , and  $\kappa$  [9,10,37] the anisotropic interaction parameter. Using 3D molecular modeler computer program [38], the molecular volume of  $\text{VO}[(\text{CH}_3)_2\text{C}=\text{NNC}(\text{SCH}_3)_2]$  was estimated to be  $370 \text{ \AA}^3$  for the cis-configuration and  $463 \text{ \AA}^3$  for the trans-configuration. From the slope of  $\tau_R$  vs  $\eta/T$ , value of  $\kappa$  can be calculated as follows:

for the trans-configuration:

$$\kappa = \frac{2.01 \times 10^{-6} \times 1.381 \times 10^{-16}}{463 \times (10^{-8})^3} = 0.599$$

for the cis-configuration:

$$\kappa = \frac{2.01 \times 10^{-6} \times 1.381 \times 10^{-16}}{370 \times (10^{-8})^3} = 0.750$$

#### 4.3.2 VO[5-MeO Sal SB](Phen)

Using the ABC program values of  $\tau_R$  for VO[5-MeO Sal SB](Phen) in methylene chloride at different temperatures were obtained. The values of  $\tau_R$  obtained are shown in Table 4.7. Fig. 4.18 presents  $\tau_R$  as a function of  $\eta/T$  for the spectra taken at higher temperatures, i.e. above the freezing point of methylene chloride. It is found that  $\tau_R$  is linear in  $\eta/T$ . Values of the viscosity of methylene chloride at different temperatures were obtained from the International Critical Table [36]. The slope of  $\tau_R$  vs  $\eta/T$  for VO[5-MeO Sal SB](Phen) at 9.47 GHz is found to be  $2.968 \times 10^{-6}$  sec  $KP^{-1}$ . For ellipsoid molecule this correlation time can be expressed in terms of Stokes-Einstein relation (Eq.4.15).

The molecular volume of VO[5-MeO Sal SB](Phen) was estimated to be  $520 \text{ \AA}^3$  using 3D molecular modeler computer program [38]. From the slope of  $\tau_R$  vs  $\eta/T$ , (Fig. 4.18).

$$\kappa = \frac{2.968 \times 10^{-6} \times 1.381 \times 10^{16}}{520 \times (10^8)^3} = 0.788$$

**Table 4.7:**  $\tau_R$  and  $\eta/T$  Values for VO[5-MeO Sal SB](Phen)  
in methylene chloride at different temperatures

T (K)	$\eta/T$ (PK <sup>-1</sup> )	$\tau_R$ (sec)
285.0	$1.657 \times 10^{-6}$	$4.835 \times 10^{-11}$
278.3	$1.820 \times 10^{-6}$	$5.320 \times 10^{-11}$
276.1	$1.878 \times 10^{-6}$	$5.500 \times 10^{-11}$
270.5	$2.042 \times 10^{-6}$	$5.980 \times 10^{-11}$
267.7	$2.134 \times 10^{-6}$	$6.250 \times 10^{-11}$
254.4	$2.643 \times 10^{-6}$	$7.765 \times 10^{-11}$
250.4	$2.832 \times 10^{-6}$	$8.320 \times 10^{-11}$
248.7	$2.918 \times 10^{-6}$	$8.581 \times 10^{-11}$
243.2	$3.220 \times 10^{-6}$	$9.492 \times 10^{-11}$
240.5	$3.389 \times 10^{-6}$	$9.980 \times 10^{-11}$
231.4	$4.072 \times 10^{-6}$	$12.00 \times 10^{-11}$

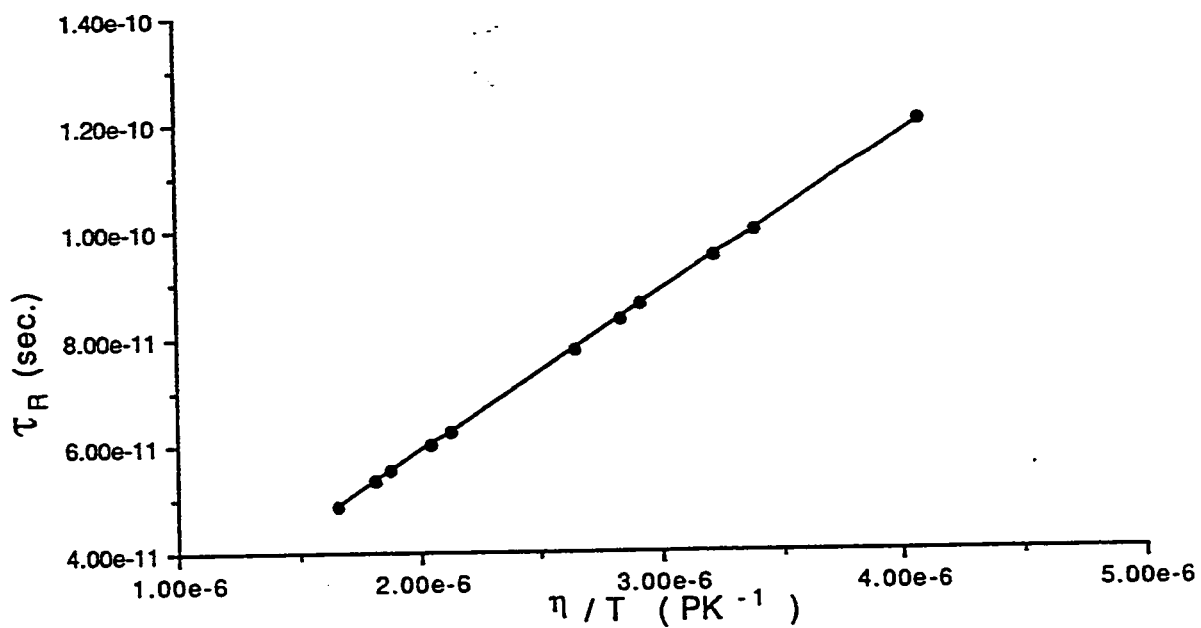


Fig.4.18 :  $\tau_R$  vs  $\eta/T$  plot for VO[5-MeO Sal SB] (Phen) in methylene chloride.



#### 4.4 STICKINESS FACTOR (S)

##### 4.4.1 VO[(CH<sub>3</sub>)<sub>2</sub>C=NNCSSH<sub>3</sub>]<sub>2</sub>:

The data above can be analyzed in terms of hydrodynamic free space model for molecular relaxation in liquids [37], a theory based on the existence of free space in the hydrodynamic continuum in which the molecule can rotate. The trans-VO[(CH<sub>3</sub>)<sub>2</sub>C=NNCSSH<sub>3</sub>]<sub>2</sub> is nearly a symmetric top with major axis  $r_{||} = 4.8 \text{ \AA}$  and minor axis  $r_{\perp} = 2.2 \text{ \AA}$  estimated using the 3D molecular modeler program [38]. Under stick boundary conditions, where the fluid at the surface of the rotating body sticks to it [39], the dimensionless rotational friction coefficient can be calculated from Perrin's formula [40]:

$$f_{\text{stick}}^{\perp} = \frac{(2/3)|1 - (\alpha^{\perp})^4|}{\frac{|2 - (\alpha^{\perp})^2|(\alpha^{\perp})^2}{|1 - (\alpha^{\perp})^2|^{\frac{1}{2}}} \ln \left| \frac{1 + |1 - (\alpha^{\perp})^2|^{\frac{1}{2}}}{\alpha^{\perp}} \right| - (\alpha^{\perp})^2} \quad (4.16)$$

where  $\alpha^{\perp}$  is symmetry parameter,  $\alpha^{\perp} = r_{\perp} / r_{||} = 0.458$ . This gives

$f_{\text{stick}}^{\perp} = 1.639$ . The corresponding value of the dimensionless rotational

friction coefficient under slip boundary condition,  $f_{\text{slip}}^{\perp}$ , is calculated from:

$$f_{\text{slip}}^{\perp} = f_{\text{stick}}^{\perp} \left[ 1 - \left( f_{\text{stick}}^{\perp} \right)^{\frac{2}{3}} \right] \quad (4.17)$$

and is found to be 0.460.

From the relationship:

$$f_{\text{slip}}^{\perp} = f_{\text{stick}}^{\perp} C_{\text{slip}}^{\text{hyd}} \quad (4.18)$$

$$C_{\text{slip}}^{\text{hyd}} = 0.460/1.639 = 0.281$$

$C_{\text{slip}}^{\text{hyd}}$  is a result of hydrodynamic calculation in which a large spheroidal object rotates in a continuous, homogeneous fluid.

In a similar way these values can be obtained for the cis-configuration of  $\text{VO}[(\text{CH}_3)_2\text{C}=\text{NNC}(\text{SSCH}_3)_2]$  :

$$r_{\perp} = 2.5 \text{ \AA}$$

$$r_{\parallel} = 4.4 \text{ \AA}$$

$$\alpha_{\perp} = 0.568$$

$$f_{\text{stick}}^{\perp} = 1.345$$

$$f_{\text{slip}}^{\perp} = 0.241$$

$$C_{\text{slip}}^{\text{hyd}} = 0.179$$

Now, how much does rotational relaxation in liquids depend upon molecular geometry and how much upon the specific nature of rotor solvent interactions?. In other words, how much of the rotational relaxation in liquids is due to hardcore interactions between rotor and solvent and how much to other interactions? To some extent, these questions can be answered by analyzing the molecular reorientational data obtained from magnetic resonance experiments. Magnetic resonance data are chosen because of the spin correlation on neighbouring molecules in dilute solutions of the paramagnetic molecules insures that the reorientational correlation times are single particle correlation times. The extent to which probe-solvent interactions occur, in hydrodynamic models, is measured by the stickiness parameter (S) [9-11] which indicates the effect on rotational relaxation by all non-hardcore anisotropic interactions.

The stickiness factor, S, is independent of molecular geometry and is

zero in the slip limit and 1 in the stick limit. For truly hydrodynamic situation  $0 \leq S \leq 1$ , but since the molecular reorientation is nonhydrodynamic, negative values of (S) are possible. The stickiness factor for the  $\text{VO}[(\text{CH}_3)_2\text{C}=\text{NNC}(\text{SSCH}_3)_2]$  at 9 GHz can be calculated using equation (1.1).

For the trans-configuration:

$$S = \frac{0.599 - 0.281}{1 - 0.179} = 0.442$$

And for the cis-configuration:

$$S = \frac{0.750 - 0.179}{1 - 0.179} = 0.695$$

The  $\kappa$  value obtained for the trans structure was compared with the  $\kappa$  value for vanadyl acetylacetonate (VOAA) in toluene ( $\kappa = 0.600$ ) [32] and found to be of exactly the same order of magnitude. The stickiness factor, S, obtained for the trans structure  $\text{VO}[(\text{CH}_3)_2\text{C}=\text{NNC}(\text{SSCH}_3)_2]$  in toluene, was compared with that calculated for VOAA in toluene ( $S = 0.449$ ) and found to be of the same order. This agreement lends further support to our conclusion that the structure of  $\text{VO}[(\text{CH}_3)_2\text{C}=\text{NNC}(\text{SSCH}_3)_2]$  is trans.

#### 4.4.2 VO[5-MeO Sal SB](Phen):

VO(5-MeO Sal SB)(Phen) is a prolate ellipsoid with major axis  $r_{||} = 5.6 \text{ \AA}$  and minor axis  $r_{\perp} = 3.2 \text{ \AA}$  as estimated using 3D molecular modeler computer program [38]. using Perrin's formula (Eq. 4.16):

$$\alpha_{\perp} = 0.571,$$

$$f_{\text{stick}}^{\perp} = 1.339$$

and

$$f_{\text{slip}}^{\perp} = 0.237$$

is calculated as done for the VO[(CH<sub>3</sub>)<sub>2</sub>C=NNCSSH<sub>3</sub>]<sub>2</sub>. This gives

$$C_{\text{slip}}^{\text{hyd}} = 0.237/1.339 = 0.177. \text{ The value of the stickiness factor,}$$

S, at 9 GHz is:

$$S = \frac{\kappa - C_{\text{slip}}^{\text{hyd}}}{1 - C_{\text{slip}}^{\text{hyd}}} = \frac{0.788 - 0.177}{1 - 0.177} = 0.742$$

It seems that VO[5-MeO Sal SB](Phen) in methylene chloride is experiencing more stickiness behavior than VO[(CH<sub>3</sub>)<sub>2</sub>C=NNC<sub>3</sub>H<sub>7</sub>SSCH<sub>3</sub>]<sub>2</sub> in toluene. These results can be understood on a molecular level since VO[5-MeO Sal SB](Phen) is a corrugated sphere capable of exerting more torque when it rotates than VO[(CH<sub>3</sub>)<sub>2</sub>C=NNC<sub>3</sub>H<sub>7</sub>SSCH<sub>3</sub>]<sub>2</sub> which is nearly a symmetric top.

#### 4.5 STOKES-EINSTEIN MODEL

The anisotropy for rotation ( $N$ ), defined earlier as  $N = R_{\parallel}/R_{\perp}$  is related to the geometric structure factor by means of the Stokes-Einstein equation [7]:

$$R_i = k_B T / (8\pi \eta r_{\parallel}^3 \sigma_i), \quad i = \parallel \text{ or } \perp \quad (4.19)$$

$$N = R_{\parallel}/R_{\perp} = \sigma_{\perp}/\sigma_{\parallel} \quad (4.20)$$

where

$$\sigma_{\parallel} = \frac{2}{3} \lambda^2 (1+\lambda^2) \left[ (1+\lambda^2) \lambda^{-1} \tan^{-1} \lambda - 1 \right]^{-1} \quad (4.21)$$

$$\sigma_{\perp} = \frac{2}{3} \lambda^2 (2+\lambda^2) \left[ (1-(1-\lambda^2) \lambda^{-1} \tan^{-1} \lambda) \right]^{-1} \quad (4.22)$$

and  $\lambda$  is a dimensionless structure factor,

$$\lambda = \frac{(r_x^2 - r_z^2)}{r_z} \quad (4.23)$$

The trans-configuration of  $\text{VO}[(\text{CH}_3)_2\text{C}=\text{NNC}(\text{SCH}_3)_2]$  is nearly a symmetric top with  $r_z = 2.2 \text{ \AA}$ ,  $r_x = 4.3 \text{ \AA}$  and  $r_y = 5.4 \text{ \AA}$  as estimated using 3D molecular modeler computer program [38]. Therefore,

$$\lambda = 1.939$$

$$\sigma_{\parallel} = 0.0780$$

$$\sigma_{\perp} = 0.160$$

and

$$N = \sigma_{\perp}/\sigma_{\parallel} = \frac{0.160}{0.0780} = 2.05$$

which is consistent, within experimental error, with our observation that  $N = 2.5 \pm 0.5$ .

The cis-configuration of  $\text{VO}[(\text{CH}_3)_2\text{C}=\text{NNC}(\text{SCH}_3)_2]$  is symmetric top with  $r_z = 2.5 \text{ \AA}$ ,  $r_x = 4.2 \text{ \AA}$ , and  $r_y = 4.7 \text{ \AA}$  as estimated using the 3D molecular modeler program.



Therefore,

$$\lambda = 1.448$$

$$\sigma_{\parallel} = 0.0367$$

$$\sigma_{\perp} = 0.133$$

and

$$N = \sigma_{\perp} / \sigma_{\parallel} = \frac{0.133}{0.0367} = 3.26$$

which is not consistent with our experimental observation,  $N = 2.5 \pm 0.5$ .

The comparison of the anisotropy for rotation,  $N$ , for the cis- ( $N = 3.26$ ) and the trans- ( $N = 2.05$ ) configurations calculated by the Stokes-Einstein equation above with our experimental value ( $N = 2.5 \pm 0.5$ ) suggests that the trans-configuration is the probable one.

Again, the agreement of  $N$ , estimated by Stokes-Einstein equation [7] using the monomer trans-configuration with our experimental  $N$  value suggests the absence of any kind of dimerization in solution. Thus ruling out the possibility of the dimeric structure through sulfur bridges which was expected since the sixth coordination position can sustain the attachment of a ligand and since the sulfur atom of the S-methyl-carbodithioato-hydrazine ligand may simultaneously bond to two

metal ions to form a bridge [1].

VO[5-MeO Sal SB](Phen) is symmetric top with  $r_z = 3.2 \text{ \AA}$ ,  $r_x = 4.3 \text{ \AA}$  and  $r_y = 6.8 \text{ \AA}$  as estimated using the 3D molecular modeler computer program [38]. For which:

$$\lambda = 2.062$$

$$\sigma_{||} = 0.0917,$$

$$\sigma_{\perp} = 0.174$$

and

$$N = \sigma_{\perp} / \sigma_{||} = 0.174 / 0.0917 = 1.90$$

which is consistent, within experimental error, with our observation that  $N = 1.7 \pm 0.5$ .

#### 4.6 ALLOWED-VALUES EQUATION

Now we want to estimate the anisotropy for rotation and the axis of rotation using the Allowed-Values Equation (AVE) [8]:

$$A \rho_x = B \rho_y + C \quad (4.24)$$

where

$$A = (\Delta A - 3\delta A) \left[ (\gamma/\beta)(\Delta \bar{g} - 3\delta \bar{g}) - \left(\frac{5}{16}\right)(\Delta A - 3\delta A) \right] \quad (4.25)$$

$$B = (\Delta A + 3\delta A) \left[ \left(\frac{5}{16}\right)(\Delta A + 3\delta A) - (\gamma/\beta)(\Delta \bar{g} + 3\delta \bar{g}) \right] \quad (4.26)$$

$$C = 4\Delta A \left[ \left(\frac{5}{16}\right)\Delta A - (\gamma/\beta)\Delta \bar{g} \right] \quad (4.27)$$

$$\Delta A = A_z - \left(\frac{1}{2}\right)(A_x + A_y) \quad (4.28)$$

$$\delta A = \left(\frac{1}{2}\right)(A_x + A_y) \quad (4.29)$$

$$\Delta \bar{g} = \left[ g_z - \left(\frac{1}{2}\right)(g_x + g_y)(\beta_o H_o/\hbar) \right] \quad (4.30)$$

$$\delta\bar{g} = \left(\frac{1}{2}\right)(g_x - g_y)(\beta_0 H_0/\hbar) \quad (4.31)$$

$$\rho_x = R_x/R_z \quad (4.32)$$

$$\rho_y = R_y/R_z \quad (4.33)$$

where  $R_x$ ,  $R_y$  and  $R_z$  are the rotational diffusion constants along the molecular X-, Y- and Z-axes respectively.

$\gamma$  and  $\beta$  are the experimental line width parameters, defined earlier as B and C in Eq. (1.23).

For isotropic reorientation  $R_x = R_y = R_z$ .

For VO[(CH<sub>3</sub>)<sub>2</sub>C=NNCSSCH<sub>3</sub>]<sub>2</sub> using the g and A tensors from the first part of this chapter and  $\gamma/\beta = 0.674$ , AVE gives:

$$\rho_x = 0.864 \rho_y - 1.153$$

The solution of the equation above is not consistent with isotropic reorientation. However, one solution of the equation may be:

$$\rho_x = 1$$

and  $\rho_y = 2.49$

which is consistent with  $N = 2.49$  along the Y-axis, which agrees with our experimental observation of  $N = 2.5 \pm 0.5$  with  $\bar{Z} = Y$ .

Similarly, for VO[5-MeO Sal SB](Phen) using the magnetic parameters from the first part of this chapter and  $\gamma/\beta = 0.690$ , AVE gives:

$$\rho_x = 0.661 \rho_y + 0.104$$

with

$$\rho_x = 1.00$$

and

$$\rho_y = 1.36$$

This is consistent with  $N = 1.36$  and  $\bar{Z} = Y$ , which agrees with our experimental results of  $N = 1.7 \pm 0.5$  with  $\bar{Z} = Y$ .

## CHAPTER FIVE

## CONCLUSION

## CHAPTER 5

### CONCLUSION

EPR line width study was carried out as a function of temperature for bis(S-methyl-3-isopropylidenehydrazinecarbodithioato)oxovanadium(IV),  $\text{VO}[(\text{CH}_3)_2\text{C}=\text{NNCSSCH}_3]_2$ , in toluene. The magnetic parameters of  $\text{VO}[(\text{CH}_3)_2\text{C}=\text{NNCSSCH}_3]_2$  in toluene were determined from the analysis of the rigid limit spectrum at 77K. An analysis employing anisotropic rotational diffusion in the fast-motion limit (when nonsecular terms are unimportant) suggest that  $\text{VO}[(\text{CH}_3)_2\text{C}=\text{NNCSSCH}_3]_2$  was undergoing axially symmetric rotational diffusion with  $N = 2.5 \pm 0.5$  at an axis  $\bar{Z} = Y$ , where  $N$  is the ratio of  $R_{\parallel}/R_{\perp}$  and  $R_{\parallel}$  is the rotational diffusion constant along the molecular Z-axis and  $R_{\perp}$  is the rotational diffusion constant perpendicular to the molecular Z axis. The  $N$  value obtained was compared with those calculated from the Stokes-Einstein model and the allowed-values equation (AVE) in an effort to determine whether the structure of  $\text{VO}[(\text{CH}_3)_2\text{C}=\text{NNCSSCH}_3]_2$  is cis or trans. The  $N$  value obtained experimentally is found to be consistent with that predicted by the Stokes-Einstein model ( $N = 2.1$ ) and with the obtained AVE ( $\rho_x = 0.864$   $\rho_y = 1.15$ ) of which the solution is  $\rho_x = 1$  and

$\rho_y = 2.49$  for a monomer in solution with a trans-configuration. Our results also indicate that the trans-configuration is more probable than the cis-configuration and rule out the possibility of a dimeric structure through sulfur bridges. The plot of  $\tau_R$  vs  $\eta/T$  is linear over the temperature range in the motional-narrowing region. The anisotropic parameter  $\kappa$ , determined from the plot of  $\tau_R$  vs  $\eta/T$  was found to be 0.599.  $\kappa$  is a measure of the coupling of rotational motions of the  $\text{VO}[(\text{CH}_3)_2\text{C}=\text{NNC}(\text{SCH}_3)_2]$  molecule to the translation modes of the fluid. The  $\kappa$  value obtained for the trans structure was compared with the  $\kappa$  value for vanadyl acetylacetonate (VOAA) in toluene ( $\kappa = 0.600$ ) and found to be of exactly the same order of magnitude. Molecular reorientation for  $\text{VO}[(\text{CH}_3)_2\text{C}=\text{NNC}(\text{SCH}_3)_2]$  in toluene was analyzed in terms of the hydrodynamic free space model for molecular relaxation in liquids. The stickiness factor  $S$  is independent of molecular geometry and is zero in the slip and 1 in the stick limit. The stickiness factor  $S$  was found to be 0.442 for the trans and 0.695 for the cis structure. For VOAA in toluene,  $S = 0.449$ . This agreement lends further support to our conclusion that the structure of  $\text{VO}[(\text{CH}_3)_2\text{C}=\text{NNC}(\text{SCH}_3)_2]$  is trans.

The second system studied is S-methyl-N-5-methoxy-salicylidenehydrazinecarbodithioato-phenanthrolineoxovanadium(IV),  $\text{VO}[5\text{-MeO Sal SB}](\text{Phen})$ , in methylene chloride. The magnetic parameters of  $\text{VO}[5\text{-MeO Sal SB}](\text{Phen})$  in methylene chloride were determined from the room temperature and the rigid limit (77K) spectra.



The motional-narrowing region analysis resulted in  $N = 1.7 \pm 0.5$  at an axis  $\bar{Z} = Y$  which is consistent with the  $N$  value obtained from the Stokes-Einstein model ( $N = 1.90$ ) and with the obtained AVE ( $\rho_x = 0.661 \rho_y + 0.104$ ) with  $\rho_x = 1$  and  $\rho_y = 1.36$ . The plot of  $\tau_R$  vs  $\eta/T$  is found to be linear over the temperature range in the motional-narrowing region. The anisotropic interaction parameter  $\kappa$ , determined from the plot of  $\tau_R$  vs  $\eta/T$  was found to be 0.788.  $\kappa$  is a measure of the coupling of rotational motions of the VO[5-MeO Sal SB](Phen) molecule to the translation modes of the fluid. The stickiness factor  $S$  was found to be 0.742. It seems that VO[5-MeO Sal SB](Phen) in methylene chloride is experiencing more stickiness behavior than VO[(CH<sub>3</sub>)<sub>2</sub>C=NNCSSCH<sub>3</sub>]<sub>2</sub> in toluene. These results can be understood on a molecular level since VO[5-MeO Sal SB](Phen) is a corrugated molecule capable of exerting more torque when it rotates than VO[(CH<sub>3</sub>)<sub>2</sub>C=NNCSSCH<sub>3</sub>]<sub>2</sub> which is nearly a symmetric top.

The magnetic parameters of a third system, VO[Sal SB](Phen) in toluene, were also determined in the same manner.

## REFERENCES

## LIST OF REFERENCES

1. Al-Guidhi, H.A., M.S. Thesis, Girl Colleges, Jeddah, Saudi Arabia, 1989.
2. Yen, T.F., Tyman, E.C. and Vaughan, G.B. In Spectroscopy of Fuels, Friedel, R.A., Ed.; Plenum: New York, 1970, 187.
3. Wilson, R. and Kivelson, D., J. Chem. Phys., 1966, **44**, , 154.
4. Hwang, J. S., Mason, R. P., Hwang, L. P. and Freed, J. H., J. Phys. Chem, 1975, **79**, 489.
5. Goldman, S.A., Bruno, G.V. and Freed, J.H., J. Phys. Chem., 1972, **56**, 716.
6. Goldman, S. A., Bruno, G. V. and Freed, J.H., J. Chem. Phys., 1973, **59**, 3071.
7. Hwang, J.S., Kivelson, D. and Plachy W., J. Chem. Phys., 1973, **58**, 1953.
8. (a) Kowert, B.A., J. Phys. Chem., 1981, **85**, 229.  
(b) Kowert, B.A., J. Phys. Chem., 1981, **85**, 1772.
9. Patron, M., Kivelson, D. and Schwartz, R. N., J. Phys. Chem. 1982, **86**, 518.
10. Kowert, B. and Kivelson, D., J. Chem. Phys., 1976, **64**, 5206.
11. Hoel, D. and Kivelson, D., J. Chem. Phys., 1975, **62**, 4535.
12. Gordy, W., Theory and Applications of Electron Spin Resonance, John Wiley & Sons, New York, 1980.

13. Pake, G. E., and Estle, T. L., *The Physical Principles of Electron Paramagnetic Resonance*, 2nd edition, 1973.
14. Carrington, A. and McLachlan, A.D., *Introduction to Magnetic Resonance*, Harper and Row, New York, 1972.
15. Freed, J. H. and Fraenkel, G. K., *J. Chem. Phys.*, 1963 **39**, 326.
16. Polnaszek, C. F. and Freed, J. H., *J. Phys. Chem.*, 1975, **79**, 2283.
17. Likhstenshtein, G. I., *"Spin Labelling Methods in Molecular Biology"*, John Wiley & Sons, New York, 1976.
18. Berliner, L. J., Ed. *Spin Labelling: Theory and Applications*, Academic Press, New York, 1976.
19. Berliner, L. J., Ed. *Spin Labelling II: Theory and Applications*, Academic Press, New York, 1979.
20. Willigen, H. V., *J. Phys. Chem.*, 1983, **87**, 3366.
21. White, L. K. and Chasteen, N. D., *J. Phys. Chem.*, 1979, **83**, No.2, 278.
22. Smith, I.C.P., Swartz, H.M., Bottom, J.R. and Borg, D.C., *Biological Applications of Electron Spin Resonance*, Edited by John Willey and Sons Inc., New York 1972.
23. Libertini, L. J. and Griffith, O .H., *J. Chem. Phys.*, 1970, **53**, 1359.
24. Campbell, R.F. and Freed, J.H., *J. Phys. Chem.* 1980, **84**, 2668.

25. Collison, D., Gohan, B. and Mabbs, F.E., J. Chem. Soc. Dalton Trans., 1987, 111.
26. Miller, G.A. and McClung, R.E.D. Inorganic Chemistry, 1973, 12, No.11, 2554.
27. Wertz, J. E. and Bolton, J. R., Electron Spin Resonance: Elementary Theory and Practical Applications, McGraw-Hill, New York, 1986.
28. Goldman, S. A., Bruno, G. V. and Freed, J. H., J. Chem. Phys., 1973, 59, 3071.
29. Freed, J. H. and Frenkel, G. K., J. Chem. Phys. 1963, 39, 326.
30. Freed, J. H. and Fraenkel, G. K., J. Chem. Phys., 1964, 40, 1815.
31. Kivelson, D., J. Chem. Phys., 1960, 33, 1094.
32. Habibur Rahman, M., M.S. Thesis, KFUPM, 1988.
33. Freed, J. H., J. Chem. Phys., 1964, 41, 2077.
34. Li, A. S. W. and Hwang, J. S., J. Phys. Chem., 1985, 89, 2556.
35. Dr. El-Sayed, L., Faculty of Science, Alexandria University, Private Communication.
36. International Critical Tables (McGraw-Hill Book Company, Inc., New York, 1930, Vol. 7, 218.
37. Dote, J. L., Kivelson, D. and Schwartz, R.N., J. Phys. Chem., 1981, 85, 2169.

38. Desktop Molecular Modeler Version 5.1.
39. Zwanzig, R. and Bixon, M., Phys. Rev., 1970, A2, 2002.
40. Dote, J.L. and Kivelson, D., J. Phys. Chem., 1983, 87, 3889.